Supplementary Figures

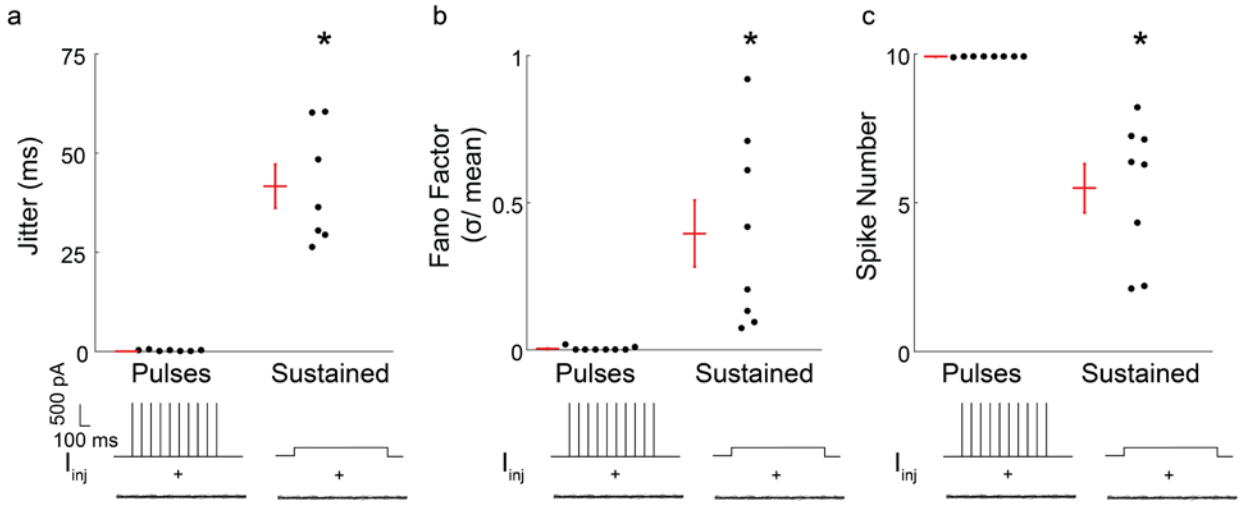

Supplementary Figure 1. Generating precise temporal sequences of action potentials requires large, rapid transmembrane current

a) Jitter of the first spike from 1 second sustained or 5 ms pulsed current injection in L2/3 pyramidal neurons near rheobase in the context of white noise injection ($p=3.1x10^{-4}$, two-sided Mann-Whitney U-Test). Bottom, schematic of current injections. Red bars indicate mean and s.e.m. for all plots (n=8 cells). Current injection amplitudes and lengths correspond to figure 1a-b (scale bar, 500 pA, 100 ms).

b) Fano factor for spike number (variance of spike number divided by the mean) for 5 ms pulses or 1 second sustained current injections over white noise ($p=1.6x10^{-4}$, Mann-Whitney U-Test, n = 8 cells).

c) Mean spike number generated from 10 x 5 ms pulsed or 1 second sustained current injections over white noise ($p=1.6x10^{-4}$, Mann-Whitney U-Test, n = 8 cells).

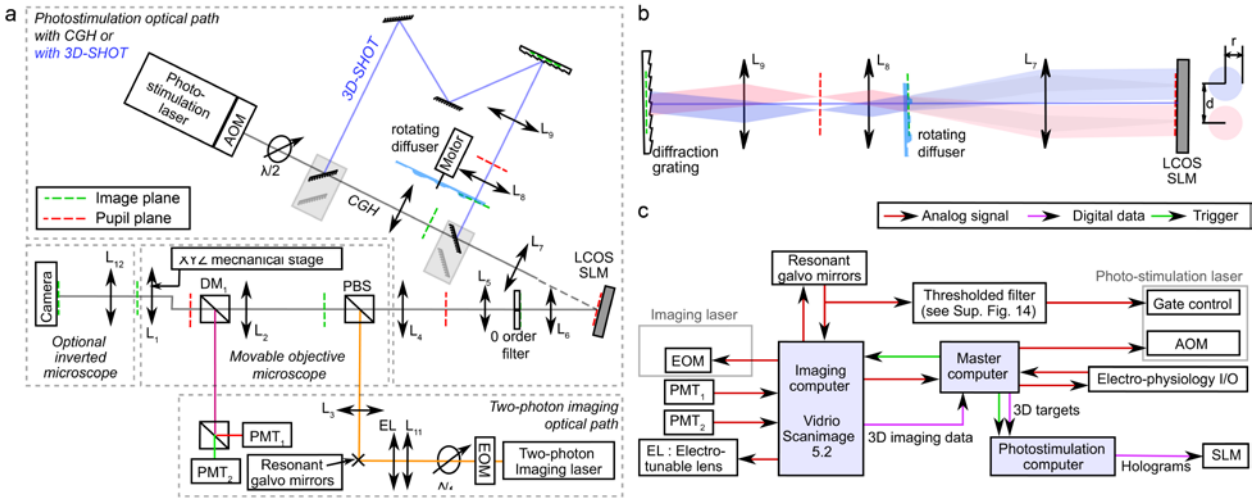

Supplementary Figure 2. Experimental setups

a) The experimental setup combines two optical paths with pulsed femtosecond laser sources. Two photon photostimulation is made possible with computer generated holography (CGH) or 3D-SHOT (blue path), and the desired modality can be selected with two sliding mirrors. For two photon imaging, a diffraction limited spot is rapidly scanned in 3D. A resonant galvomirror system enables 2D scanning in the image plane while an electro-tunable lens enables focusing at the desired depth. Imaging and photostimulation are efficiently merged into the optical path of the microscope with a polarizing beam splitter. One polarization carries the laser beam for two photon imaging, while the orthogonal polarization is used for photostimulation.

b) 3D-SHOT relies on a diffraction grating to split femtosecond pulses into separate spectral components that propagate along slightly different directions (blue and red paths show both ends of the spectrum for illustrative purposes). Spectrally separated pules coherently recombine in virtual images of the diffraction grating (dashed green lines). The diffraction grating spatial frequency determines the amount of spectral separation (distance d on the SLM). To maximize diffraction efficiency by the SLM placed in the pupil plane (red dashed lines), 3D-SHOT requires a phase pattern to be applied to the temporally focused object. In this new implementation of 3D-SHOT, we rely on a rotating holographic diffuser to randomize the phase pattern in time. The diffuser characteristic angle determines the spatial expansion of all spectral components (radius *r*).

c) The imaging system is independently controlled using Vidrio Scanimage 5.2, and receives a digital trigger anytime volume image acquisition is requested. A second computer is dedicated to photostimulation, for precomputing of the holograms, and for online display of holograms on the SLM in response to a trigger pulse. Both computers are controlled by a third (master) computer that synchronizes imaging, photostimulation as well as any electro-physiology measurement, when relevant.

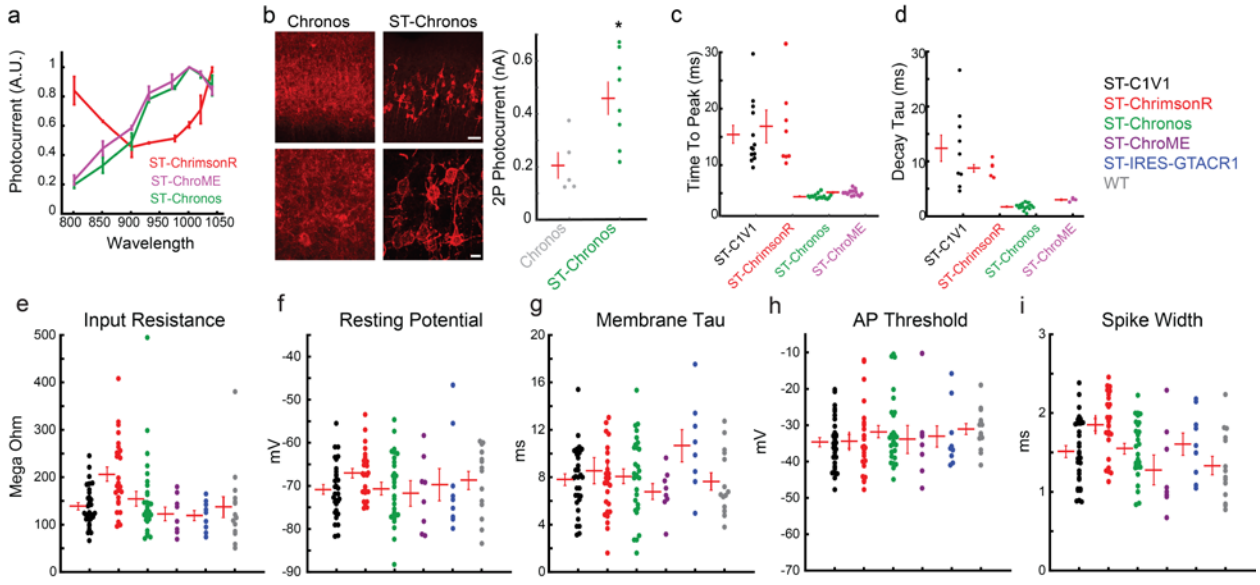

Supplementary Figure 3. Characterization of a suite of new ST-Opsins

a) Normalized photocurrent as a function 2P wavelength (at constant power) for ST-ChrimsonR (red, n=3 cells), ST-Chronos (green, n=3 cells), and ST-ChroME (purple, n=3 cells). Data are mean and s.e.m.

b) Left, representative images of brains electroporated with Chronos-mRuby2 or ST-Chronos-mRuby2 (top, 10x, scalebar = 50 µm; bottom, 60x, scalebar = 10 µm). Right, current amplitudes elicited by 2P CGH stimulation of L2/3 pyramidal neurons in brain slices expressing Chronos (gray) or ST-Chronos (green) (* indicates p=0.019, two-sided Mann-Whitney U-Test, data are mean and s.e.m. of n =5 Chronos-mRuby2 expressing neurons and n = 8 ST-Chronos-mRuby2 expressing neurons).

c) Quantification of latency from stimulation onset to peak current amplitude for 2P CGH stimulation at 0.04 mW/um^2 (20 mW, data are mean and s.e.m. from n = 13 neurons for ST-C1V1$_{T/T,}$ n = 8 neurons for ST-ChrimsonR, n = 15 neurons from ST-Chronos, and n = 13 neurons for ST-ChroME).

d) Quantification of primary decay tau from 2P CGH stimulation at 0.04 mW/um^2 (20 mW, data are mean and s.e.m. from n = 9 neurons for ST-C1V1$_{T/T,}$ n = 5 neurons for ST-ChrimsonR, n = 15 neurons from ST-Chronos, and n = 5 neurons for ST-ChroME).

e) Input resistance of L2/3 neurons electroporated with the ST-C1V1 $_{T/T}$ (black, n = 31 neurons), ST-ChrimsonR (red, n = 29 neurons), ST-Chronos (green, n = 26 neurons), ST-ChroME (magenta, n = 21 neurons), ST-IRES-eGTACR1 (blue, n = 9 neurons), or WT (gray, n = 14 neurons). Red bars indicate mean and s.e.m.

f) Resting potentials (mV) of L2/3 pyramidal neurons electroporated with the indicated constructs.

g) Membrane tau (ms) of electroporated L2/3 pyramidal neurons.

h) Action potential threshold (mV) of electroporated L2/3 pyramidal neurons.

i) Spike width (ms) of electroporated L2/3 pyramidal neurons.

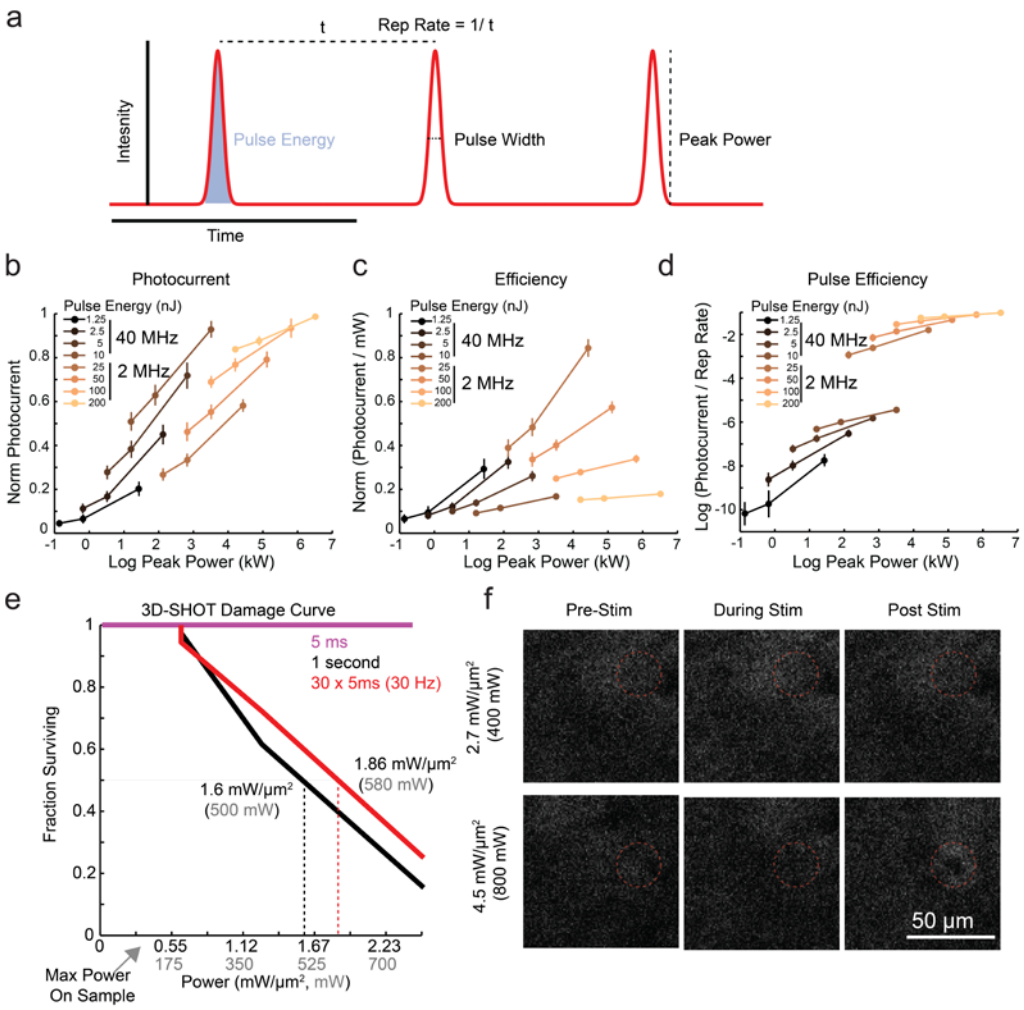

Supplementary Figure 4. Shaping 2P stimulation laser pulses for safe, efficient excitation

a) Schematic of laser pulse properties that were varied in this experiment.

b) Data showing the relationship between the laser pulse peak power and normalized photocurrent. Colored lines indicate the pulse energy, which was spread across different rep rates. Peak power was manipulated by changing either average power via the EOM (each line is a separate average power) or by altering the pulse width (pulse width varies smoothly within lines). Data represent mean ± s.e.m. of n = 8 neurons expressing ST-Chronos.

c) As in b, but plot of laser pulse efficiency, defined as normalized photocurrent per mW of average power leaving the microscope objective.

d) As in a, but plotting the Log photocurrent elicited per laser pulse (Norm. photocurrent divided by Rep. Rate).

e) Cumulative curve showing the fraction of neurons that were undamaged by high power 3D-SHOT stimulation for one 5 ms pulse (magenta), one 1 sec pulse (black) or thirty 5 ms pulses at 30 Hz (red). LD50s are indicated with dashed lines. Data are from n = 39 neurons in N = 2 CamkII-tTA, teto-GCaMP6s animals.

f) Representative example of experiment quantified in (e) of high power 1 second stimuli pre (left), during (middle), or post (right) stimulation for stimuli that did not cause damage (top) or resulted in damage (bottom, dashed red circle indicates holographic target, scalebar = 50 µm).

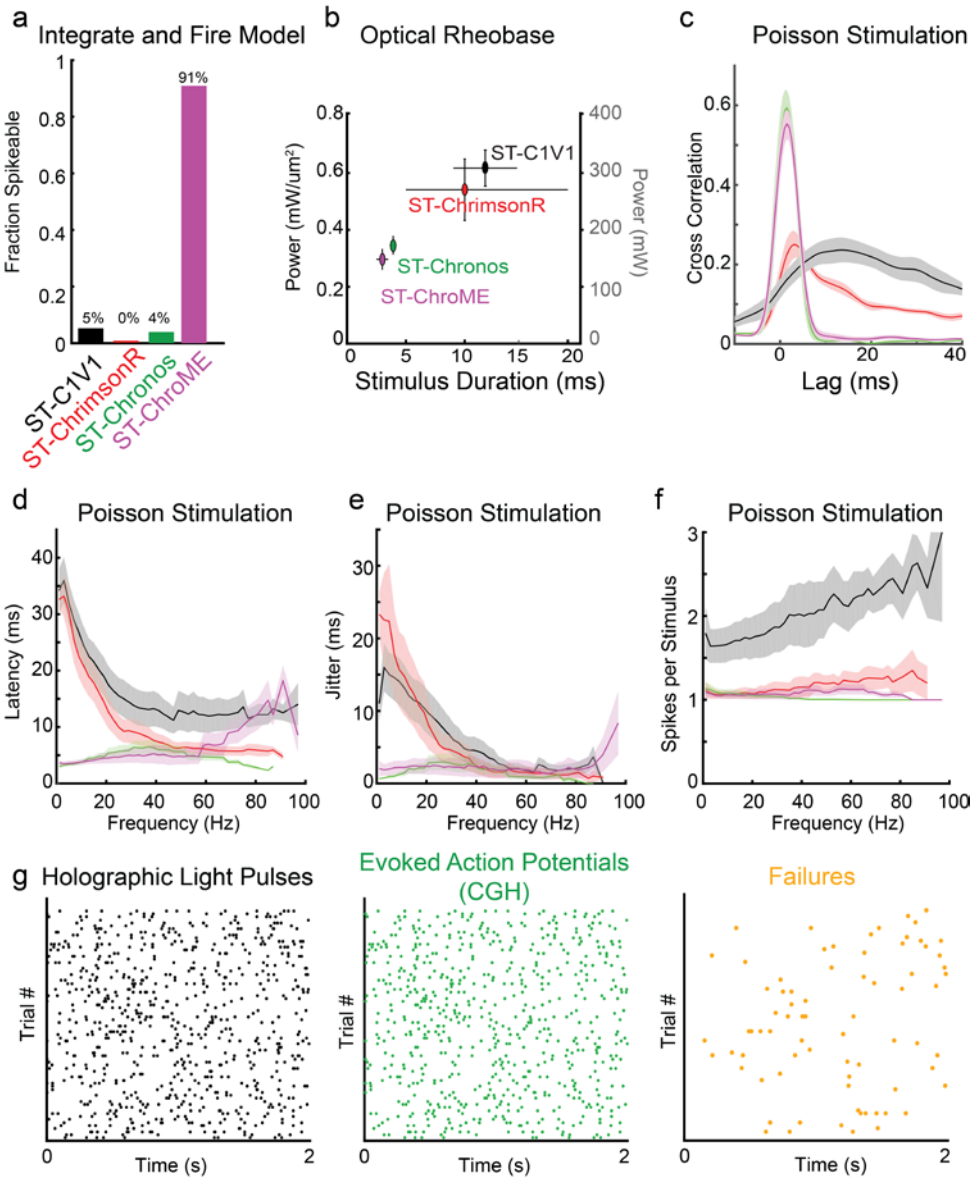

Supplementary Figure 5. Poisson stimulation of ST-Opsins in brain slices

a) Results from an integrate and fire model of a typical L2/3 neuron using the amplitude, rise, and decay taus for the photocurrents recorded in Fig 1c (CGH, 5ms, 0.4 mW/µm^2, 200 mW) to predict whether they could generate action potentials in a model L2/3 pyramidal neuron.

b) Scatter plot indicating the mean and s.e.m. of the optical rheobase (e.g. the combination of laser power and stimulus duration needed to elicit action potentials) from ST-Opsin-expressing L2/3 pyramidal neurons in brain slices (ST-C1V1 $_{T/T}$: n=8 neurons; ST-Chronos: n = 26; ST-ChrimsonR: n=5; ST-ChroME: n = 8).

c) Cross correlation of Poisson CGH light pulses and recorded action potentials for neurons expressing each neuron in brain slices (data represent mean and s.e.m., ST-C1V1 $_{T/T}$: n=7 neurons; ST-Chronos: n = 4; ST-ChrimsonR: n=4; ST-ChroME: n = 7).

d) Latency to spike as a function of instantaneous stimulus frequency during Poisson stimulation. Data represent the mean and s.e.m. (ST-C1V1: n=7, ST-ChrimsonR: n=5, ST-

Chronos: n=9, ST-ChroME: n =7). Data was binned in 2 Hz bins displayed as a 5 Hz rolling average.
e) As in c, jitter as a function of instantaneous frequency during Poisson stimulation (jitter was calculated as the standard deviation of the latencies in each time bin).
f) As in c and d, but plotting the number of spikes occurring within a 5 ms window after a holographic stimulus as a function of instantaneous stimulus frequency during Poisson stimulation.
g) An example Poisson stimulation experiment from a L2/3 pyramidal neuron expressing ST-ChroME. Left, black dots indicate 2P CGH light pulses. Middle, green dots indicate light-evoked action potentials. Right, orange dots indicate failures.

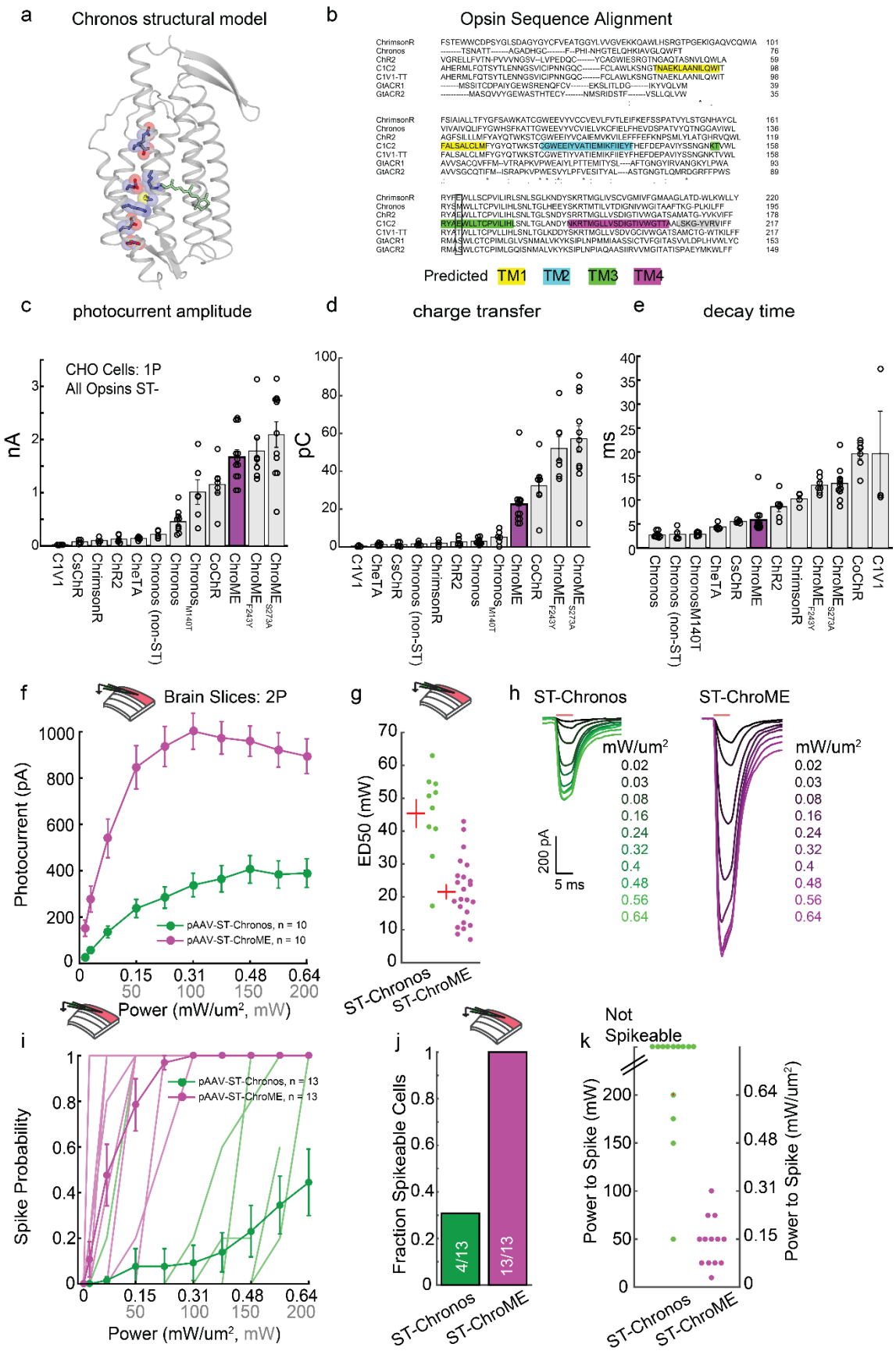
a
Chronos structural model
b
Opsin Sequence Alignment
ChrimsonR
Chronos
ChR2
C1C2
C1V1-TT
GtACR1
GtACR2
Predicted TM1 TM2 TM3 TM4
c
photocurrent amplitude
CHO Cells: 1P
All Opsins ST-
nA
C1V1
CsChR
ChrimsonR
ChR2
CheTA
Chronos (non-ST)
Chronos
Chronos M140T
CoChR
ChroME
ChroME F243Y
ChroME S273A
d
charge transfer
pC
e
decay time
ms
ChronosM140T
f
Brain Slices: 2P
Photocurrent (pA)
pAAV-ST-Chronos, n = 10
pAAV-ST-ChroME, n = 10
Power (mW/um², mW)
g
ED50 (mW)
ST-Chronos
ST-ChroME
h
ST-Chronos
ST-ChroME
mW/um²
0.02
0.03
0.08
0.16
0.24
0.32
0.4
0.48
0.56
0.64
200 pA
5 ms
i
Spike Probability
pAAV-ST-Chronos, n = 13
pAAV-ST-ChroME, n = 13
Power (mW/um², mW)
j
Fraction Spikeable Cells
4/13
13/13
k
Not Spikeable
Power to Spike (mW)
Power to Spike (mW/um²)

Supplementary Figure 6. Mutagenesis to generate ST-ChroME

a) Structural model of the Chronos pore region guided by the C1C2 crystal structure.

b) Opsin sequence alignment with putative transmembrane regions highlighted; the M140 residue that we mutated in Chronos is highlighted with a black box.

c) Photocurrents recorded via 1P stimulation of CHO cells for each opsin at 0.55 mW (470 nm unless otherwise indicated). Data indicate the mean and s.e.m. of ST-C1V1 $_{T/T}$ (n=5, 550 nm), ST-CsChR (n=5), ST-ChrimsonR (n=5, 630 nm), ST-ChR2 (n = 6), ST-CheTA (n = 6), Chronos (n = 10), ST-Chronos (n = 11), ST-Chronos$_{M140T}$ (n = 21), ST-CoChR (n = 7), ST-Chronos$_{F243Y}$ (n = 14), ST-ChroME (n = 19), ST-ChroME$_{S273A}$ (n = 18).

d) Charge transfer from the neurons shown in (c).

e) Decay Tau calculated from the data shown in (c).

f) Power curve showing photocurrents recorded in voltage clamp in response to 5 ms 3D-SHOT stimulation of increasing power for ST-Chronos (green, n = 10) or ST-ChroME expressed via AAV infection (magenta, n = 10, data represent mean and s.e.m.).

g) ED50 for 2P stimulation from ST-ChroME (n = 23) or ST-Chronos (n = 10, p = 2,14x10^{-4}, two-sided Mann Whitney U-Test, red bars denote mean and s.e.m.).

h) Average traces for ST-Chronos and ST-ChroME for increasing power levels (as in panel f, color codes from dark to bright correspond to increasing power levels).

i) Spike probability for neurons recorded in current clamp virally expressing ST-Chronos (n=13) or ST-ChroME (n = 13) as a function of pulses of increasing power. Data represent mean and s.e.m. for the population, with individual neuron traces overlaid.

j) Quantification of the number of cells that could be spiked in (g) at power levels below 200 mW (0.64 mW/um^2) when virally infected with ST-Chronos or ST-ChroME.

k) Scatter plot showing the power level needed to spike each cell expressing ST-Chronos or ST-ChroME via viral infection.

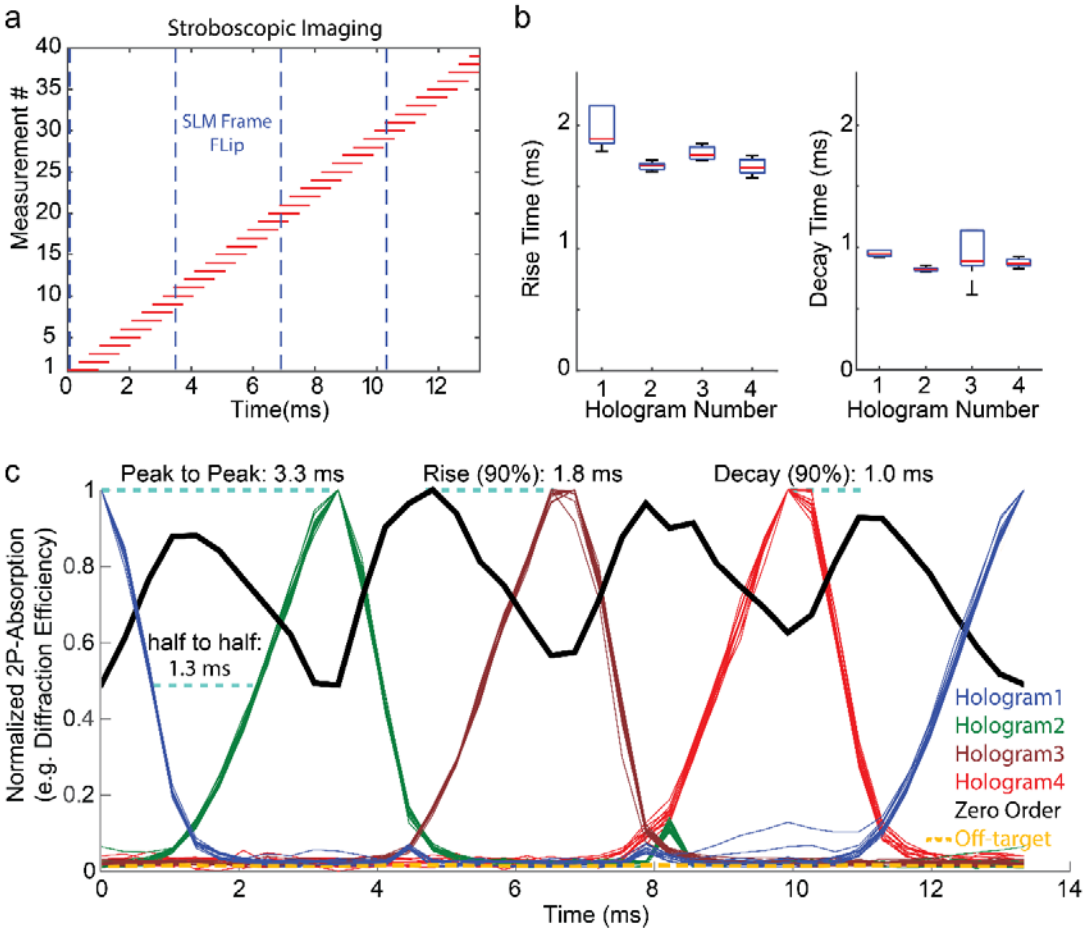

Supplementary Figure 7. Quantifying SLM Speed

a) High-speed stroboscopic imaging sequence. Four holograms are displayed in a repeating cycle. Dashed blue lines indicate SLM frame flip at 300Hz. Each 1 ms red line indicates the time period which laser was on (and therefore fluorescence sampled) for 40 linearly distributed measurements along the duration of the cycle (*y*-axis).

b) Left, quantification of the transition time to 90% peak 2P absorption (e.g. diffraction efficiency) for 4 multi-spot holograms. Right, quantification to 90% decay. Box plots show mean (red bar), quartiles (blue box), and range (black bars). Data represent n = 3 measurements of N = 10 spots per multi-target hologram.

c) Quantification of the 2P absorption (e.g. diffraction efficiency) of four holograms (colored lines) flipped at 300 Hz on the Meadowlark 512L SLM. Black line indicates 2P absorption detected in the zero-order, which was unblocked for this measurement. Peak-to-peak, half-to-half, and rise and decay times are indicated with dashed teal lines. Individual colored lines show the signal in each target of the multi-spot holograms. Yellow dashed line indicates light detected in all non-targeted areas normalized to the maximal 2P absorption in all targets. When the SLM flips, absorption rapidly decays in the first set of targets, then increases within the second set. During transition, light falls within the zero-order, which is normally blocked, and no two-photon absorption was detected in non-targeted locations (see Supplementary movie 1).

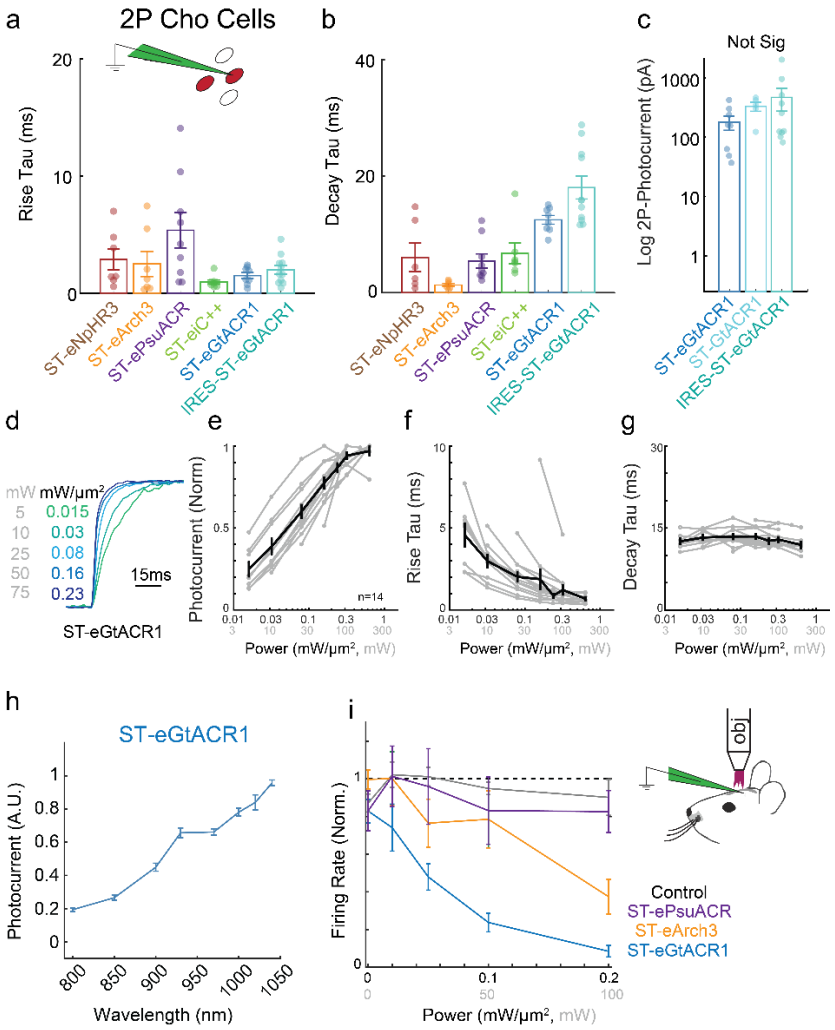

Supplementary Figure 8. eGTACR Kinetics

a) Quantification of 2P rise kinetics from photocurrents from CHO cells expressing one of several different opsins. Photocurrents were elicited with 500 ms 0.2mW/µm^2 (100 mW) photostimulation. Data represented as mean and s.e.m. with each dot from a different cell. (n=7 ST-eNpHR3, n=7 ST-eArch3, n=9 ST-ePsuACR, n=8 ST-eiC++, n=8 ST-eGtACR1, n=11 IRES-ST-eGtACR1).

b) Quantification of 2p decay kinetic as in (a).

c) Comparison of photocurrents elicited from CHO cells expressing ST-eGtACR1, IRES-ST-eGtACR1, or ST-GtACR1 (Note: ST-eGtACR1 and IRES-ST-eGtACR1 photocurrents are also presented in figure 2b; n=8 ST-eGtACR1, n=10 IRES-ST-eGtACR1, n=5 ST-GtACR1, presented as mean and s.e.m.).

d) On rate of a ST-eGtACR1 photocurrent in a CHO cell with a variety of different stimulation intensities, and normalized to the same depolarization. Note the on kinetic is dependent on stimulation intensity. Scalebar = 15 ms.

e) Quantification of photocurrents as a function of stimulation intensity normalized to the peak photocurrent observed for each CHO cell. Data is pooled between all tested GtACR1 constructs. (n=14 cells, presented as mean and s.e.m.)

f) Quantification of rise kinetic as a function of stimulation intensity as in (f).
g) Quantification of decay kinetic as a function of stimulation intensity as in (f).
h) Normalized photocurrent as a function 2P wavelength (at constant power) for ST-eGtACR1 (data from ST-eGtACR1 and IRES-ST-eGtACR1 combined). Data represented as mean and s.e.m. (n=8 cells).
i) Quantification of power dependence of holographic suppression *in vivo.* 2P guided loose patch recordings from cells expressing ST-ePsuACR1, ST-eArch3, St-eGtACR1, or no opsin with 500 ms of stimulation. Data presented as mean and s.e.m. (n=7 no opsin control, n=6 ST-ePsuACR, n=8 ST-eArch3, and n=10 ST-eGtACR1).

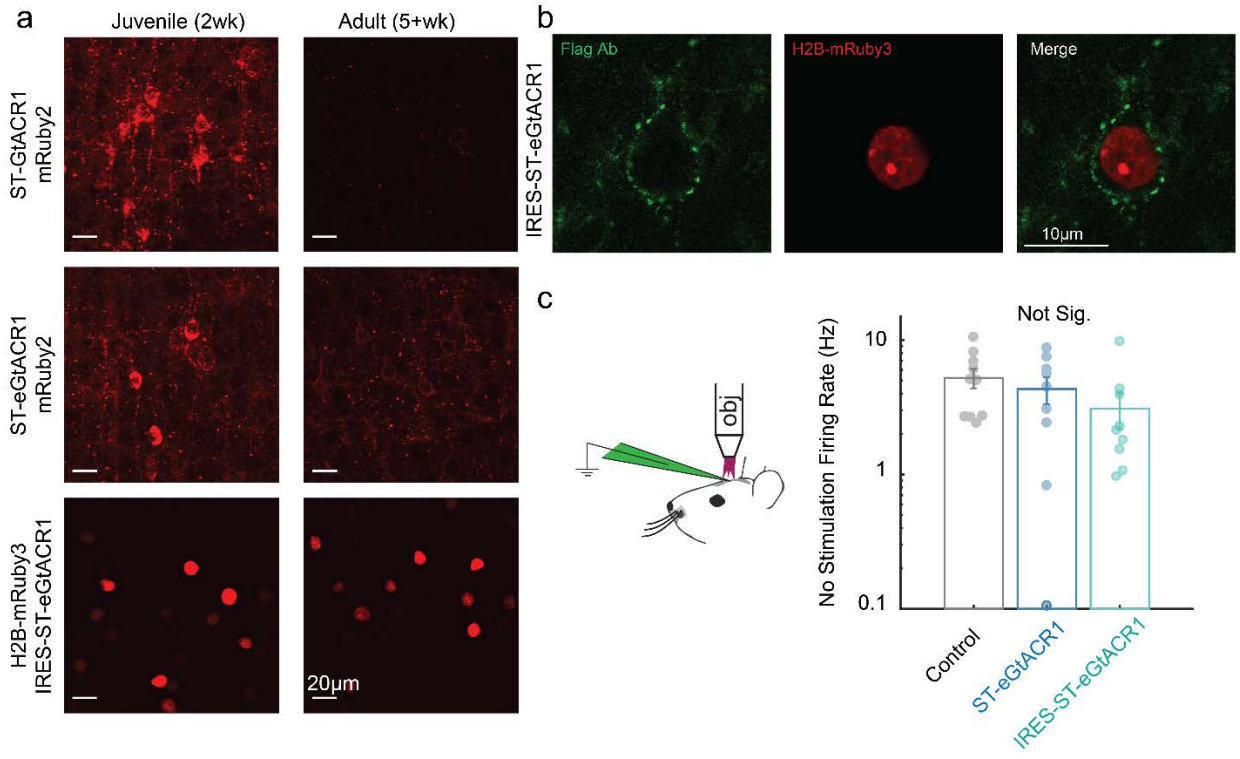

Supplementary Figure 9. GtACR1 Fluorescence Loss

a) Representative images from mice electroporated with one of three different GtACR1 constructs, taken from littermates that were 14 days old (left) or over 35 days old (right) with imaging conditions matched within each opsin. Data are representative images taken from n = 3 mice. ST-eGtACR1 and IRES-ST-eGtACR1 are the same examples as in Figure 2d zoomed out and presented here for comparison.

b) Representative image of anti-Flag antibody staining for the GtACR1 protein in IRES-ST-eGtACR1 mice. Flag staining co-localizes with mRuby3 nuclei and appear consistent with retained soma targeting. Representative image from experiment independently repeated in n = 3 mice.

c) Left, schematic of experimental configuration. Right, plot showing that firing rates in the absence of stimulation are unaffected by the expression of ST-eGtACR1 or IRES-St-eGtACR1 (n= 10 control, n= 9 ST-eGtACR1, n= 9 IRES ST-eGtACR1, data are mean and s.e.m., p>0.1 Kruskal Wallis).

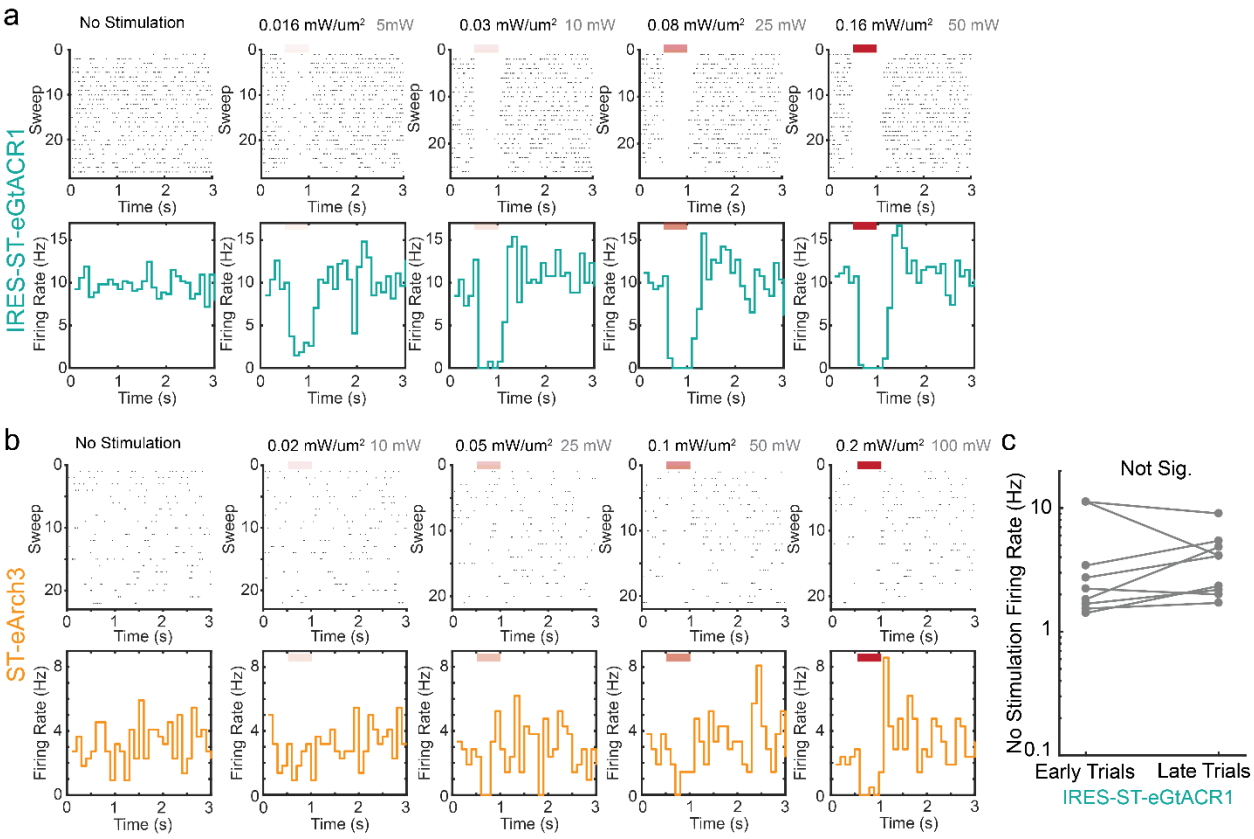

Supplementary Figure 10. *In vivo* suppression of neural activity

a) Raster plot (above) and Histogram (below) of the firing of a neuron expressing IRES-ST-eGtACR1 stimulated at a variety of stimulation intensities per Hologram. Recorded using *in vivo* 2P guided loose patch. Histograms are binned at 100 ms.

b) As in (a), but a neuron expressing St-eArch3.0.

c) Firing rates during absence of stimulation are unchanged by repeated holographic stimulation in IRES-ST-eGtACR1 expressing cells. Firing rates at the first half of a recording were not significantly different from the last half of recording (p=0.373 Wilcoxon two-sided Signed Rank Test, n = 9 mice). Recordings ranged from 28-344 trials (mean 155).

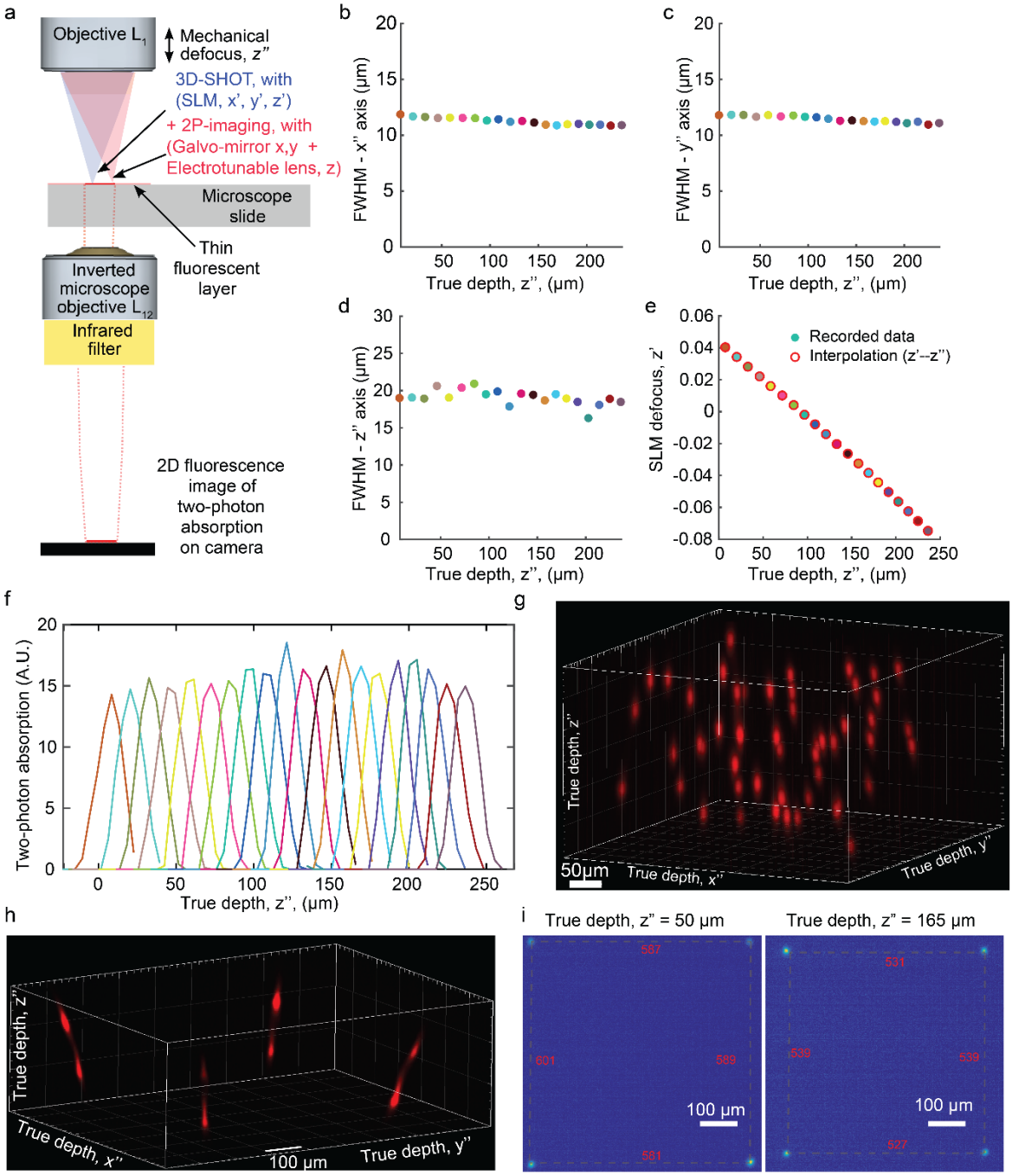

Supplementary Figure 11. Characterization of 3D-SHOT 2.0.

a) Volume images of two-photon induced fluorescence were recorded by placing a calibration slide coated with a thin film of fluorescent material under the microscope objective. The fluorescent film intersects the 3D photostimulation distribution at any desired depth z'' by adjusting the position of the microscope objective with the mechanical stage. An inverted microscope with a secondary camera records the two-photon induced fluorescence in 2D. By stacking 2D images while moving the objective along the z'' axis, we record direct 3D

measurements of the two-photon absorption distribution.
b-e) 30 holograms targeting a single spot at various depths were computed and the corresponding image was recorded in 3D. Measurements of the FWHM along the *x*, *y*, and *z* axis provide the characteristic dimensions of the Custom Temporally Focused Pattern (CTFP) object (12 *12 *20 μm). The size of the CTFP can be adjusted (see methods). We observe a slight dependence of the CTFP dimensions with depth that correspond to well-known variations of the effective magnification on either side of the natural focal plane of the objective. A random color code is assigned to each hologram. The center of the temporally focused pattern for each hologram was identified with Gaussian curve fitting and the depth in the coordinate system of the SLM (z') is displayed as a function of the measured true depth (z''), with the same randomized color coding. This data was used to compute a polynomial interpolation allowing rapid conversion from one system of coordinates to the other (red circles).
f) Superimposed response curves showing two photon absorption as a function of depth for each hologram. Spatial resolution is similar on both sides of the zero order of the optical system (z" = 120 μm).
g) An example hologram with 50 randomly distributed targets spanning across a 500 * 500 * 250 μm effective volume of operation. The targets are power balanced with our digital interpolation.
h) An example hologram with 8 targets placed near the corners of the 550 * 550 *100 μm volume that corresponds to the imaging window.
i) As in h, but two-plane fluorescent intensity images showing the (*x,y*) location of the corner targets. The distances between the corners are noted in red (μm).

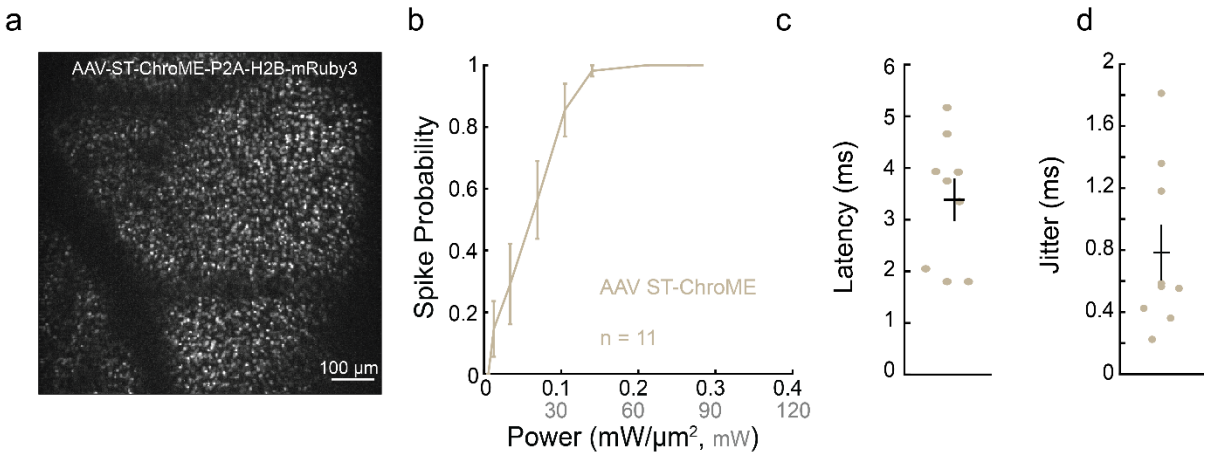

Supplementary Figure 12. Characterization of AAV CAG-DIO-ST-ChroME-P2A-H2B-mRuby3 *in vivo*

a) Maximal intensity projection of a z-stack taken in primary somatosensory cortex of an Emx-Cre mouse injected with AAV-CAG-DIO-ST-ChroME-P2A-H2B-mRuby3 (scale bar = 100 µm, representative of N = 7 animals).

b) Spike probability as a function of laser power for 1 Hz stimulation *in vivo* cell attached recordings (data are mean ± s.e.m., n = 11 neurons).

c) Latency to spike at best power for n = 11 neurons (black bars show mean and s.e.m.).

d) Spike time jitter at best power for n = 11 neurons (black bars show mean and s.e.m.).

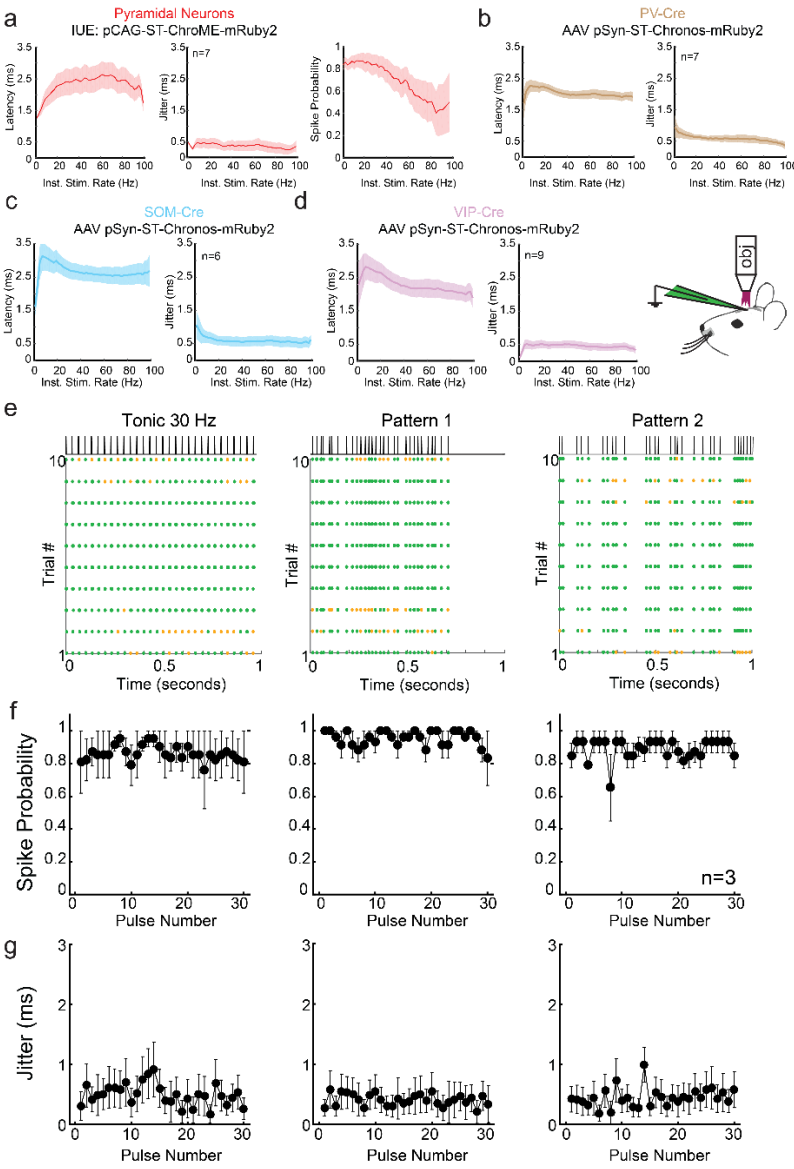

Supplementary Figure 13. 3D-SHOT Poisson stimulation of cortical neurons *in vivo*

a) Latency, jitter, and spike probability as a function of instantaneous stimulation rate during *in vivo* Poisson stimulation using 3D-SHOT for pyramidal neurons expressing ST-ChroME (n=7). Data represent mean (solid line) and s.e.m. (shaded area) of data as a function of instantaneous stimulation frequency binned with bin width 2 Hz.

b) Latency and jitter as in (a) but for PV neurons expressing ST-Chronos (n =7)

c) As in b, but for SOM neurons (n = 6)

d) As in b, but for VIP neurons (n = 9)

e) Raster plots from an example neuron showing spiking responses to three stimulus patterns, each with 30 pulses per second, but with distinct temporal structures. Top, black lines indicate light pulses; green circles denote light-evoked action potentials, and orange ticks show failures. Data show ten trials for each stimulus pattern for an example neuron.

f) Average spike probability for each stimulus pattern as a function of stimulus number for each pattern. Data represent the mean and s.e.m. of the mean values from n = 3 PV neuron recorded *in vivo*.
g) Average spike time jitter for each stimulus pattern as a function of stimulus number for each pattern. Data represent the mean and standard error of n = 3 PV neurons recorded *in vivo*.

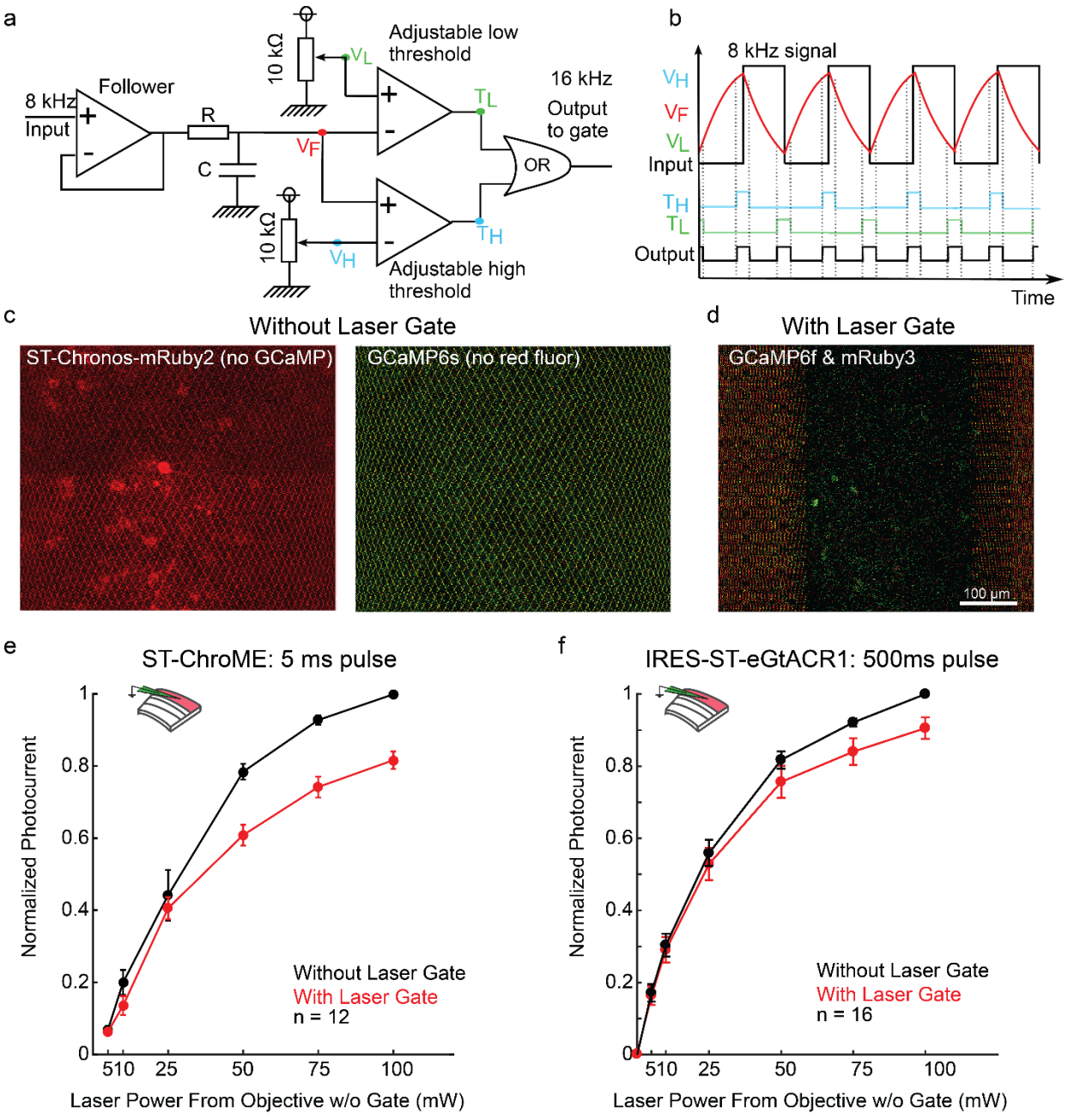

Supplementary Figure 14. A fast thresholded RC circuit for simultaneous photostimulation and imaging

a) Circuit design to synchronize imaging and photostimulation. The resonant galvomirror feedback provides a square 0-5V signal indicating the precise moment when the mirror reverses direction. The signal is first amplified with a follower circuit and serves as input to charge and discharge a capacitor, C = 2 µF, R = 170Ω. The voltage in the capacitor V_F serves as input for two threshold circuits that yield a TTL (5V) signal anytime the voltage is above resp. below a threshold value, $V_{H,}$ resp. V_L. Both thresholds can be manually adjusted with a potentiometer. An OR gate logically sums the detected high and low thresholds T_H and T_L to yield the output signal.

b) Analog and digital signals. Input signal: 8kHz square feedback signal from the resonant galvo mirror (black). Voltage in the capacitor V_F (red), and TTL threshold detection (T_L, T_H) are shown for adjustable threshold values (V_L, and V_H). The OR gate yields a 16KHz control signal that gates the photostimulation laser and restricts 3D-SHOT excitation to the period around when the resonant galvo mirror is reversing its direction, i.e. when imaging the edges of the field of view.
c) Left, representative image during holographic stimulation of neurons expressing ST-Chronos-mRuby2 without the gating circuit engaged, right representative image during holographic stimulation of GCaMP6s-expressing neurons without the RC circuit engaged (artifact masks the GCaMP6-expressing neurons). Data is representative of N = 12 animals.
d) Raw image showing holographic stimulation of PV neurons expressing GCaMP6f and IRES-GtACR1-nls-mRuby3. The image gate allows photostimulation to occur on either side of the field of view (artifacts on edge of image) while allowing imaging to remain unobstructed in the middle.
e) Whole cell voltage clamp recordings of 3D-SHOT evoked current from neurons expressing ST-ChroME without the laser gate (black) or with the laser gate circuit engaged (n = 12 neurons, 5 ms pulses, data represent mean ± s.e.m.).
f) Whole cell voltage clamp recordings of 3D-SHOT evoked current from neurons expressing IRES-ST-GtACR1 without the laser gate (black) or with the laser gate circuit engaged (n = 16 neurons, 500 ms pulses, data represent mean ± s.e.m.).

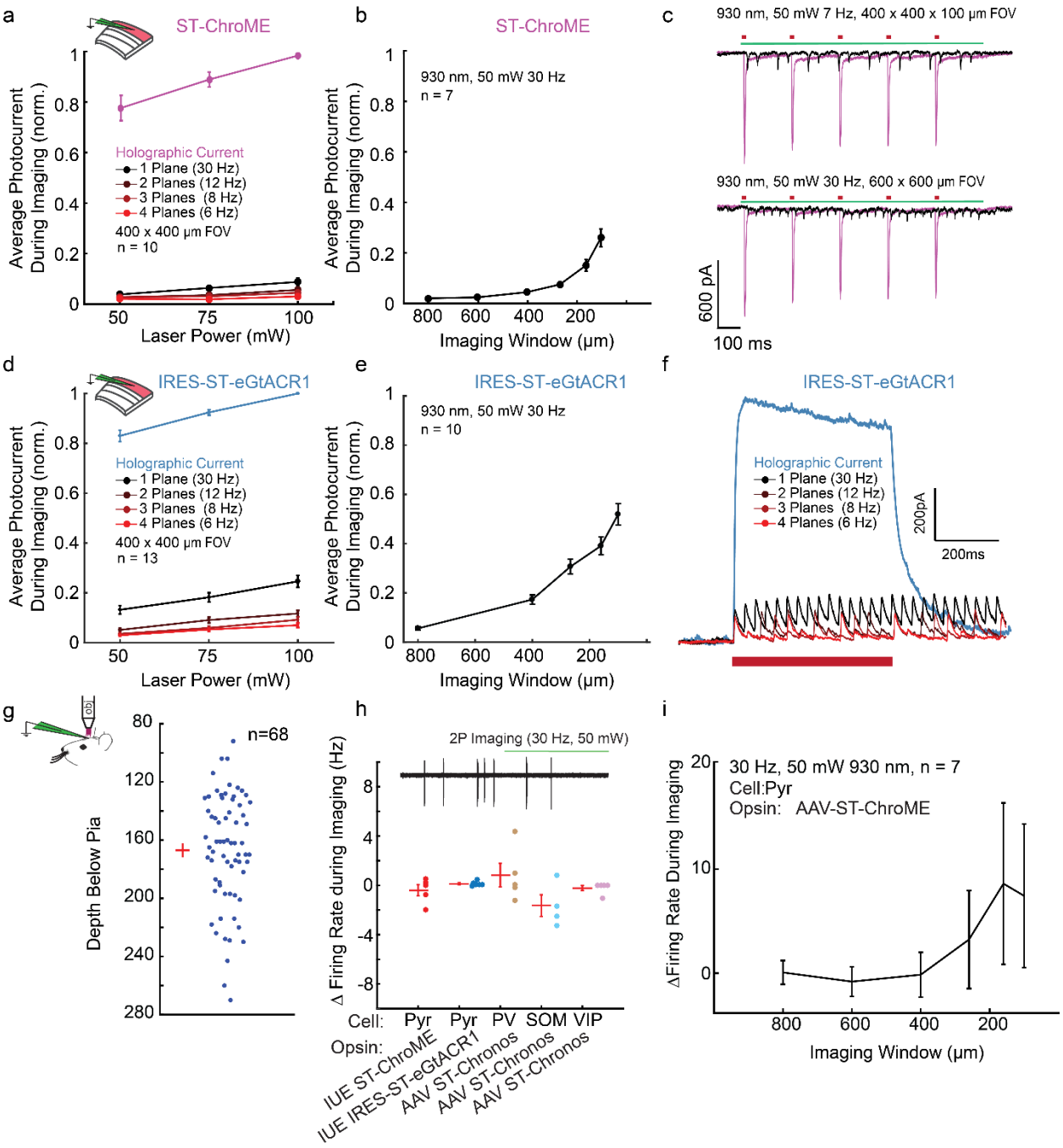

Supplementary Figure 15. Quantification of optical cross-talk due to the GCaMP6 imaging laser

a) Summary plot of voltage clamp recordings from neurons expressing AAV ST-ChroME in brain slices. For all neurons, photocurrents are normalized to the maximum observed value during the experiment. Magenta: photocurrents in response to holographic stimulation at increasing powers (1040 nm). Black through red indicate the mean imaging-evoked photocurrent over a one-second imaging period at the indicated frame rate and imaging laser power (930 nm, 400 x

400 µm field of view, imaging planes spaced 50 µm apart). Data represent the mean and s.e.m. from n = 10 neurons.
b) Imaging-evoked photocurrents as a function of imaging window size. Data are normalized to holographic currents observed shown in (a). Imaging was performed at 30 Hz, 50 mW, and 930 nm. Data represent mean and s.e.m. from n = 7 neurons).
c) Traces from an example neuron showing holographic currents (magenta) and imaging-induced photocurrents (black) evoked at 50 mW (1040 nm, 5 ms for holographic pulses, 930 nm 1 second of imaging).
d) As in a) but for L2/3 pyramidal neurons expressing AAV IRES-ST-eGtACR1 (n = 13 neurons).
e) As in b) but for L2/3 pyramidal neurons expressing AAV IRES-ST-eGtACR1 (n = 10 neurons)
f) Traces from an example neuron showing holographic currents (blue) and imaging-induced photocurrents (black through red) evoked at 50 mW (1040 nm, 500 ms for holographic pulses, 930 nm 1 second of imaging, imaging frame rate shown on figure).
g) Scatter plot showing the depths of neurons recorded from *in vivo* during 2P holographic experiment (n = 68 neurons, mean ± s.e.m. = 167±4.6 µm below pial surface).
h) Top, example traces of spiking neuron expressing ST-ChroME during initiation of 2P imaging (green bar = 3 seconds). Bottom, 2P guided i*n vivo* loose patch experiments from the indicated cell-type expressing the indicated opsin showing the mean change in firing rate before and after initiation of 2P calcium imaging (50 mW, 930 nm, 30 Hz, 400 x 400 µm single plane field of view). Red bars indicate population mean and s.e.m., n = 5 ST-ChroME expressing pyramidal neurons, n = 6 IRES-GtACR1 expressing pyramidal neurons, n = 5 ST-Chronos expressing PV neurons, n = 4 ST-Chronos expressing SOM neurons, n = 5 ST-Chronos expressing VIP neurons.
i) 2P guided *in vivo* loose patch recordings from AAV ST-ChroME pyramidal neurons showing the change in firing rate as a function of imaging window size (30 Hz, 50 mW, 930 nm, data represent mean and s.e.m. of n = 7 neurons).

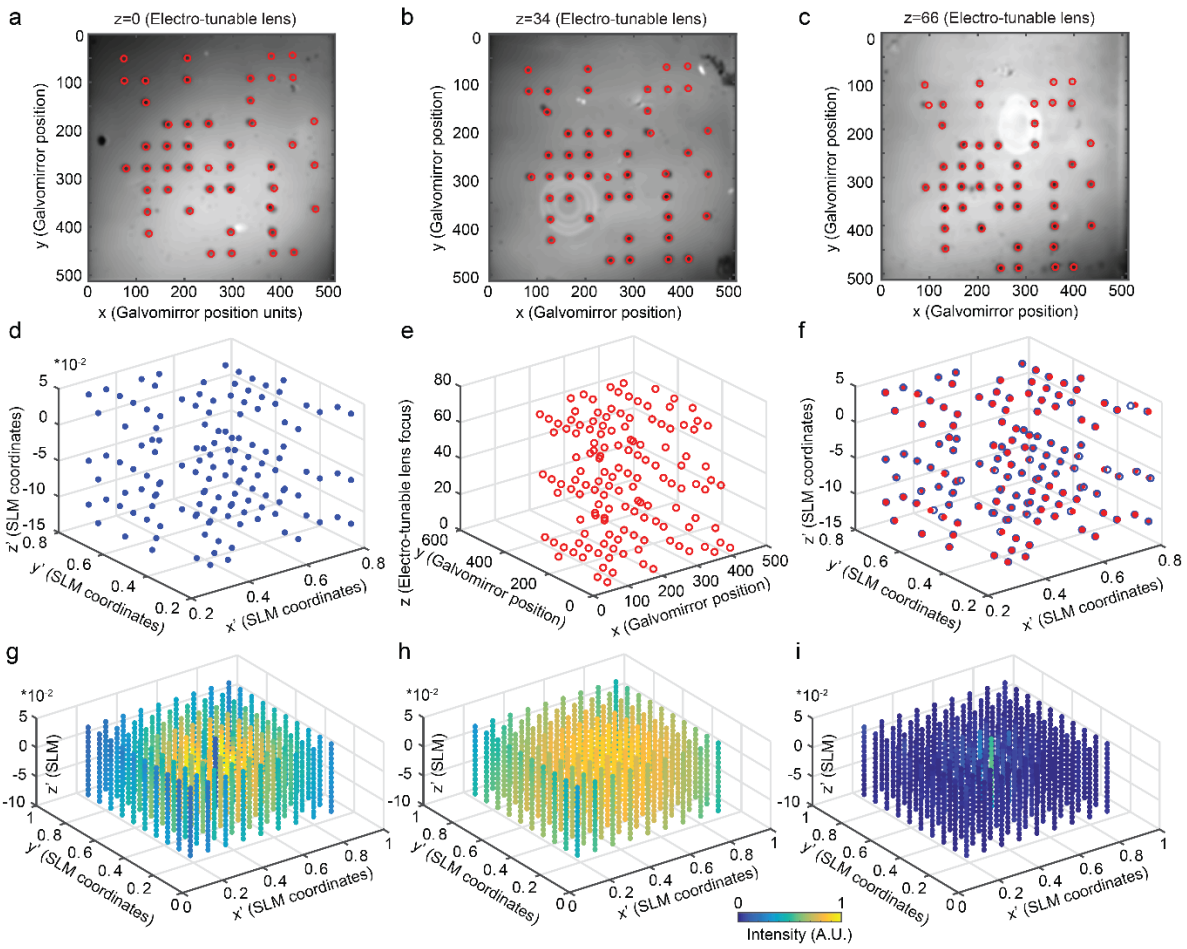

Supplementary Figure 16: 3D alignment procedure

a-c) A randomized pattern (SLM coordinates x',y',z') is engraved on the calibration slide and visualized with two-photon imaging to identify the corresponding (x,y,z) coordinates of the spots (red circles). The result is a data set of matched points for which we simultaneously know (d) the 3D coordinates in the SLM coordinates (x',y',z'), as well as (e) the corresponding locations (x,y,z) in the imaging coordinates system. We use this dataset to compute a 3D polynomial interpolation enabling rapid conversion from one system of coordinates to another.

f) Measured coordinates (in blue) are converted, and simultaneously displayed alongside known coordinates (in red) in the reference frame of the SLM to identify interpolation errors, if any.

g) Two photon absorption was measured at constant laser power for N = 9*10*15 targets in a 3D grid pattern. We display the two photon absorption in each location (normalized scale bar). The steep drop in the center of the volume corresponds to the blocked zero order of the SLM, in x'=y'=0.5.

h) Estimation of the received intensity (from the square root of the two photon absorption, normalized). We rely on this 3D polynomial interpolation to estimate losses along the optical path as a function of target location (x',y',z'). The zero-order block is ignored in the interpolant, and a separate warning reminds the user to avoid targeting near the zero order block.

i) The reconstruction error shows interpolation failures, if any.

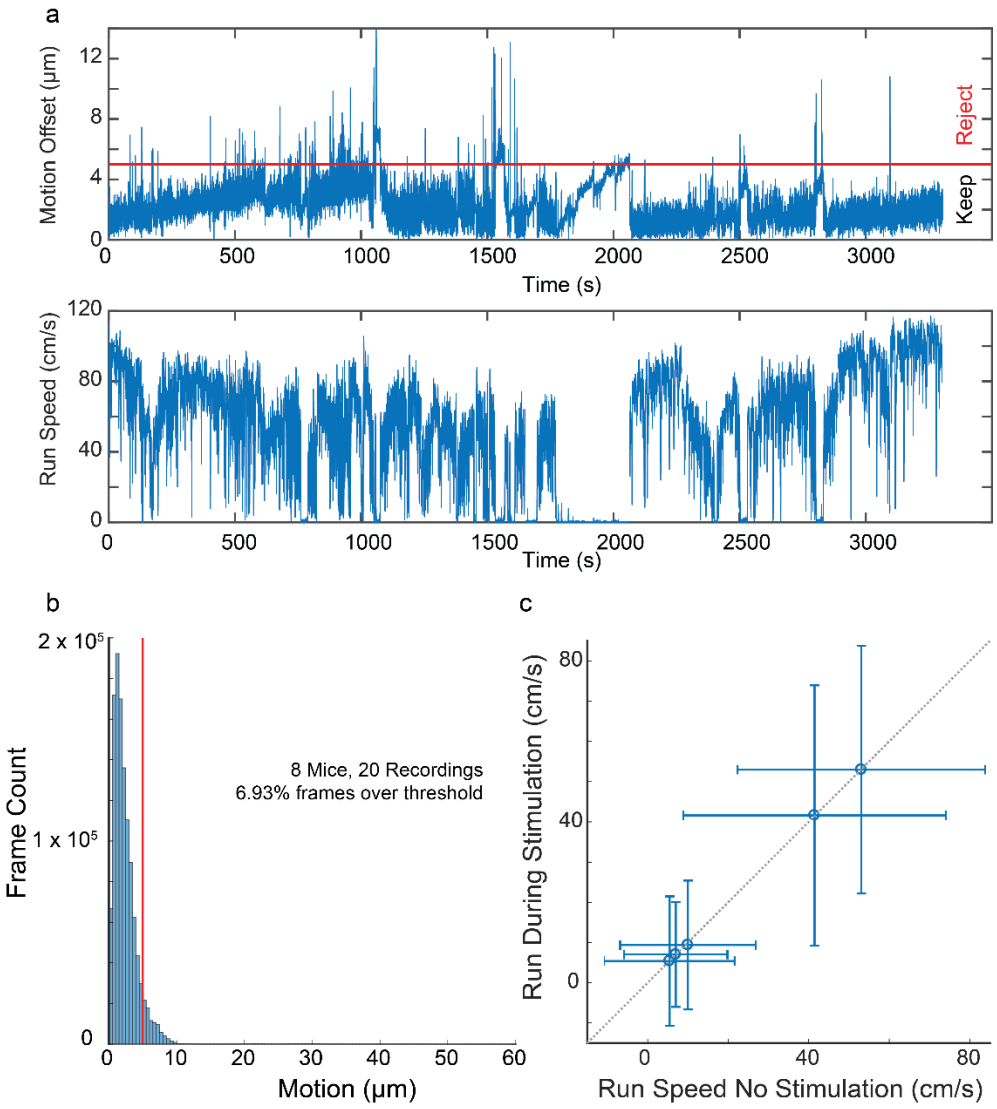

Supplementary Figure 17. Holographic stimulation does not affect running behavior or cause motion

a) Top, traces of the motion over an entire experiment (orange line represents the threshold where motion might cause failures or off-target activation). Bottom, running speed of the same animal over the entire experiment.

b) Histogram of the average motion per frame for all experiments. Data come from n = 20 volumetric recordings (3 planes each, or 60 planes) and N=8 mice, expressing either ST-ChroME or IRES-ST-eGtACR1.

c) Scatter plot of run speed of animals during 1 second holographic stimulation plotted against 1 second periods of time when holographic stimulation was not active. Each data point represents the mean and standard deviation of run speed during a recording. N=3 mice expressing IRES-ST-eGtACR1.

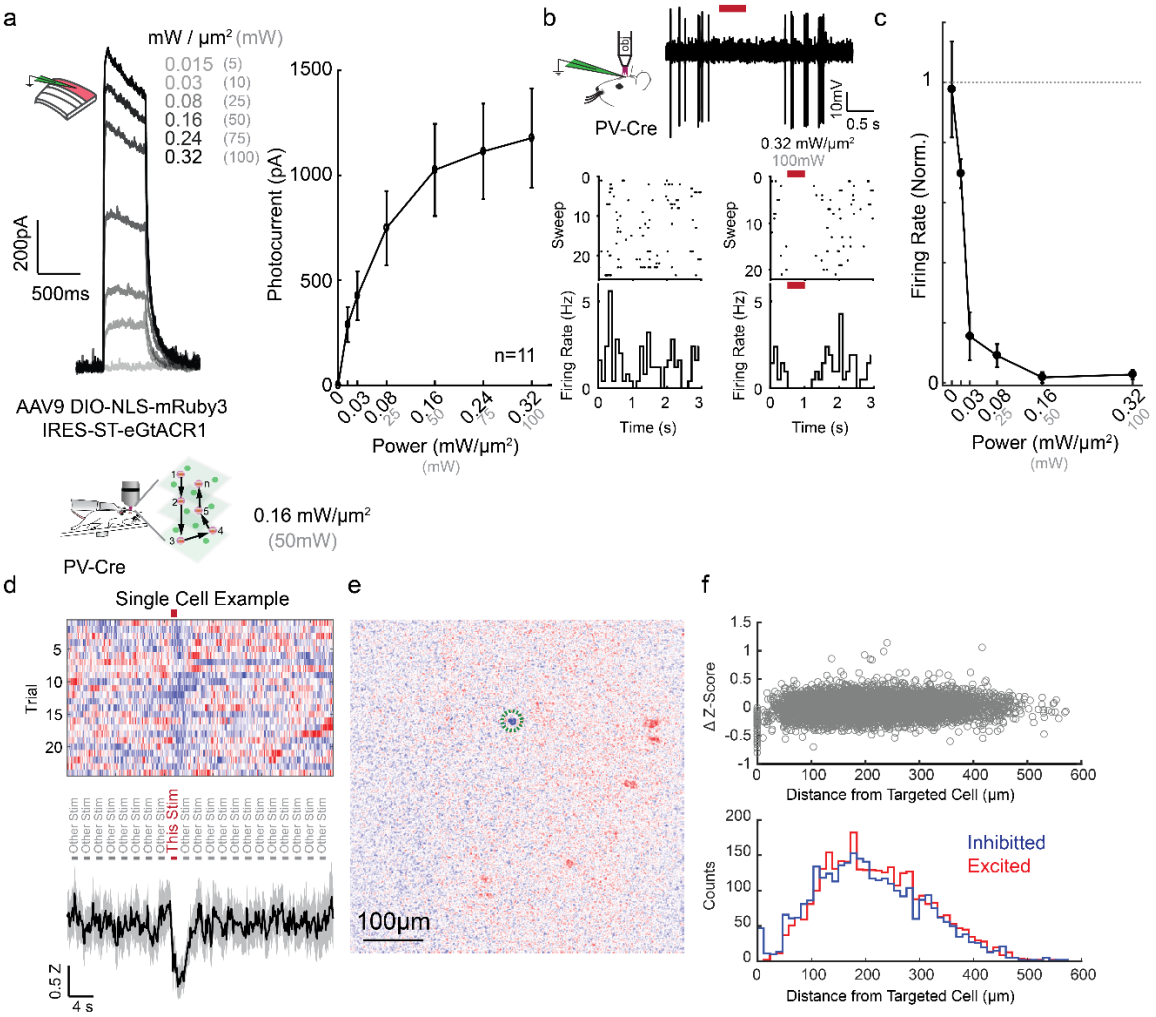

Supplementary Figure 18. Characterizing AAV IRES-ST-eGtACR1

a) Representative traces from whole cell recordings from L2/3 pyramidal neurons held at 0 mV and expressing virally delivered AAV9 NLS-mRuby3-IRES-ST-eGtACR1 (left), and summary data (right) during holographic stimulation. Maximum photocurrent 1100±220pA at 0.32mW/µm^2 (100mW, n=11 cells, presented as mean and s.e.m.).

b) Cell attached recordings from PV-Cre mice expressing virally delivered IRES-ST-eGtACR1. Representative single trial trace (top) high-pass filtered at 500 Hz, and summary raster plots (below) comparing control trials to 0.32mW/µm^2 (100mW) holographic stimulation.

c) Summary data of IRES-ST-eGtACR1 positive PV cells responding to holographic stimulation at a variety of stimulation intensities (n=3 cells, mean ± s.e.m.).

d) Top, schematic of experimental design as in Figure 6a. Middle, Z-scored fluorescence of 24 trials from a single cell across ~40 seconds of imaging, with stimulation of this cell in the middle (red bar) and 20 neighboring cells offset (grey bars). Bottom, mean ± 95% confidence interval of response to stimulation.

e) Average image of z-scored fluorescence during stimulation of the same neuron as in (d) during stimulation.

f) Top, average response of every detected neuron to the suppression of each targeted neuron (9840 interactions; 164 detected neurons x 60 targets), organized by magnitude of change in fluorescence (in Z-scored activity) vs distance from the targeted cell. Bottom, number of interactions that increased fluorescence (red) compared to those that decreased fluorescence (blue) sorted by distance from targeted cell.

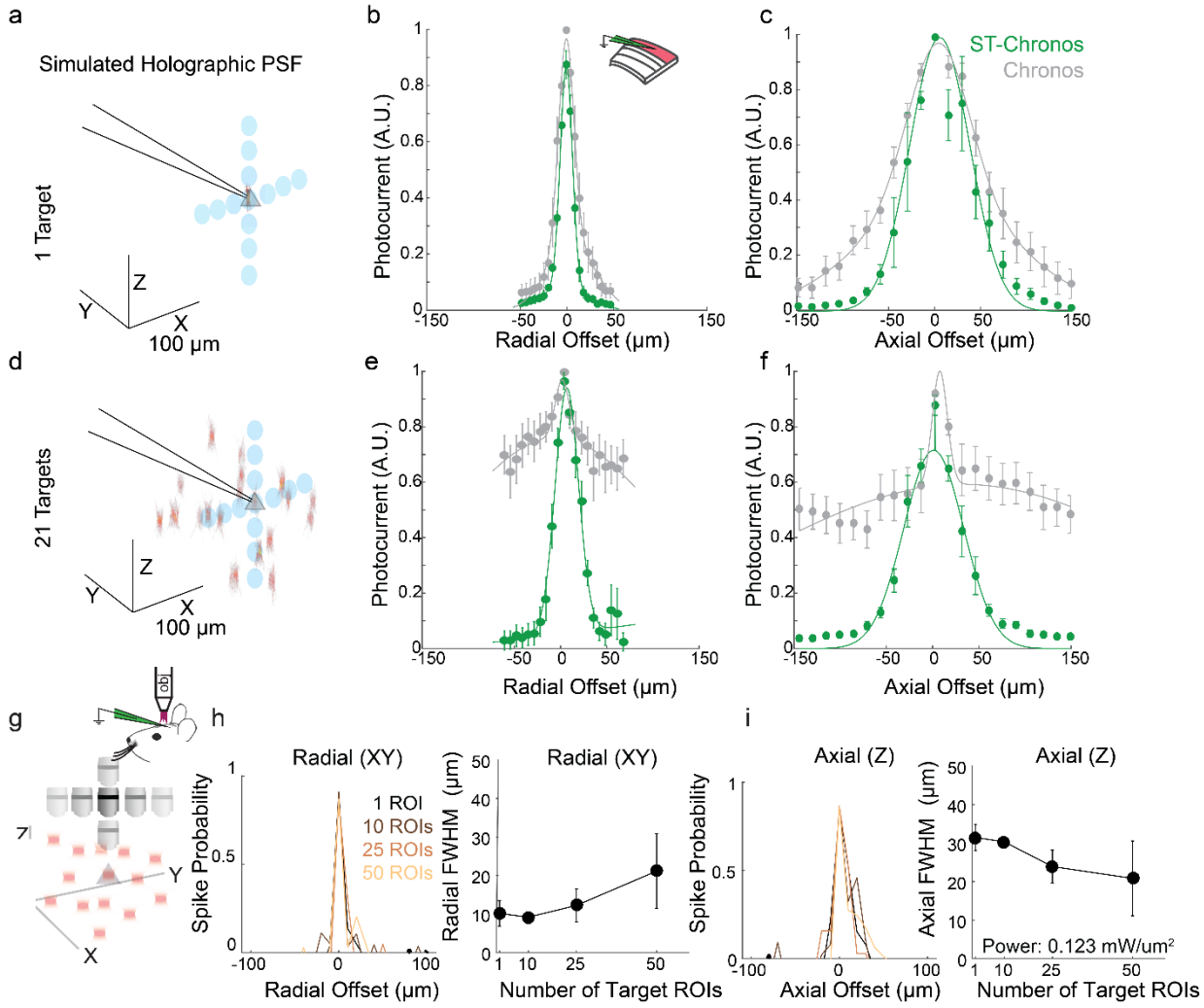

Supplementary Figure 19. Spatial Resolution during ensemble stimulation *in vivo*

a) Experimental protocol to measure the physiological point spread function (PPSF). A single-target hologram is digitally displaced radially and axially around the soma of a neuron held in voltage clamp, and the photocurrent is recorded as a function of the radial or axial displacement of the hologram.

b) Radial PPSF (photocurrents) from L2/3 neurons in brain slices expressing Chronos-mRuby2 (gray, FWHM = 33.15±5.46 µm, n =7 neurons) and for ST-Chronos-mRuby2 (green, FWHM = 21.5±5.46 µm, n =8, p=0.016, two-sided Mann-Whitney U-Test).

c) As in b, but measuring the axial PPSF (Chronos FWHM = 127±18.4 µm, n =7 neurons, ST-Chronos 76±2.69 µm, n =7, p=0.036, two-sided Mann-Whitney U-Test).

d) Experimental protocol to measure the PPSF in the context of multiple neuron stimulation. A hologram targeting 21 spots is generated with the center target on a patched neuron. Electrophysiological recordings are performed as the center spot, targeting the patched neuron, is digitally displaced axially and radially around the patched cell (others targets remain in place).

e) Radial PPSF in the context of 21 spot activation (Chronos: 153.55±29.8 µm n = 6 neurons, ST-Chronos: 37.5±11.6 µm, n=8, p=0.0012 two-sided Mann-Whitney U-Test)
f) Axial PPSF in the context of 21 spot activation; inset, FWHM of Gaussian fits (Chronos: 206.8±34.38 µm, n=4 neurons, ST-Chronos: 63±3.12 µm, n = 7, $p=5.83x10^{-4}$, two-sided Mann-Whitney U-Test).
g) Schematic of *in vivo* resolution testing in the context of stimulating 1, 10, 25, or 50 target spots with a single hologram. The hologram is held constant on the SLM while the objective is moved radially or axially to measure the spiking PPSF for each axis.
h) Left, representative neuron showing radial spiking PPSF for simultaneous 3D-SHOT stimulation of 1, 10, 25, or 50 spots. Right, quantification of radial *in vivo* 3D-SHOT FWHM as a function of target number (n=3 cells, data indicate mean and s.em.).
i) Left, representative neuron showing axial spiking PPSF for simultaneous 3D-SHOT stimulation of 1, 10, 25, or 50 spots. Right, FWHM for axial *in vivo* 3D-SHOT PPSF as a function of number of targets (n=3 cells, data indicate mean and SEM). For b and c, all holograms were targeted with constant power density (2 W, or 40 mW/target, 0.123 mW/um^2)

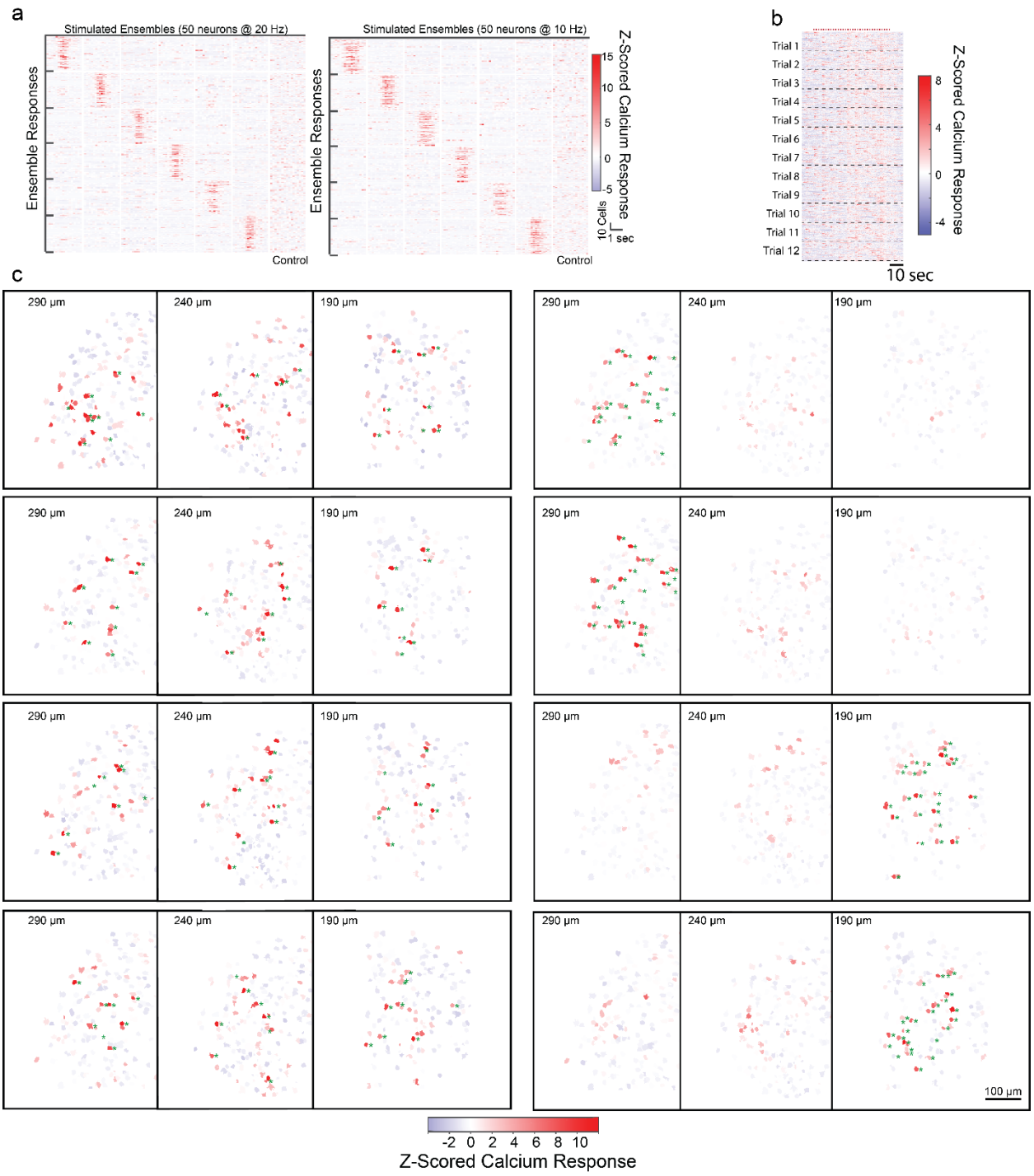

Supplementary Figure 20. Spatiotemporally precise ensemble stimulation

a) Left, example raster plots showing the mean z-score of the deconvolved calcium activity for six ensembles of 50 neurons each (rows) when each of them are stimulated with ten x 5 ms pulses at 20 Hz (columns). The last column is a control stimulation where 50 random spots in the field of view are targeted. Right, the same, but for ten x 5ms pulses at 10 Hz. Data are mean values from a representative experiment (N = 3 mice).

b) Single-trial calcium rasters of the z-scored dF/F for a sample ensemble of 50 neurons. Data are the single-trial z-scored calcium response for each of the neurons in the artificially selected ensemble over 12 trials (separated by dashed lines). Note that during the course of the experiment neurons are repetitively stimulated as parts of different groups of cells over the course of the experiment.
c) Average z-scored deconvolved calcium response for 3D-SHOT stimulation of 8 unique ensembles stimulated simultaneously, 25 neurons each. Calcium sources are segmented and color coded based on the z-scored deconvolved calcium activity for 200 ms after stimulation (see color bar on bottom). Neurons that were stimulated are marked by a green asterisk.

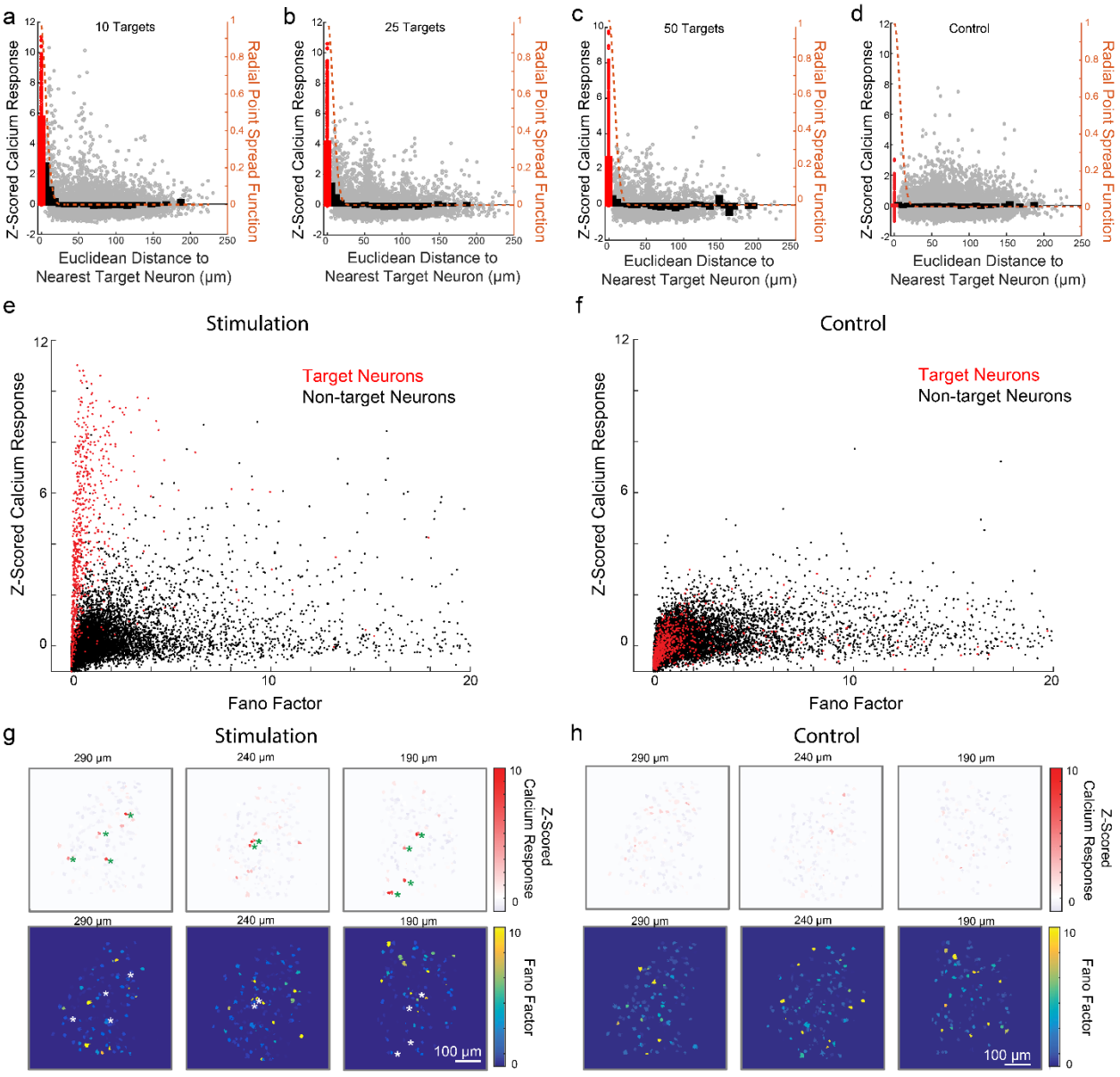

Supplementary Figure 21. Spatial Resolution During Ensemble Stimulation

a) Z-scored response to stimulation as a function of the distance to the nearest holographic photostimulation target for 10-target holograms in awake, running animals, from Figure 7. Data from all 10-target holograms in a representative experiment are superimposed. Red dots are targeted neurons, and gray dots are non-target neurons. The binned mean response to stimulation is shown in black bars. The PPSF measured with a patch electrode is superimposed in orange: neurons located 0-11.5 μm away from stimulation targets exhibit average facilitation consistent with direct activation with the laser (z-score = 1.6±2.2 mean and s.d., n = 212, p = $3x10^{-19}$, one-sided t-test), but neurons just outside the PPSF (11.5-24.5 μm) show no evidence of off-target light (z-score: 0.08±0.98, n = 427, p=0.09, one-sided t-test). Neurons located greater than 30 μm away from a target cell exhibit suppression (z-score: -0.11±0.68, n = 6606, p=$1.94x10^{-35}$, one-sided t-test). Note that the cluster of cells around 50 and 100 μm away

reflects the 50 µm spacing between z-planes, so there are many more neurons located around 50 or 100 µm away from the nearest target cell.
b) As, in (a), but for 25-target holograms. Neurons located 0-11.5 µm away from stimulation targets: z-score = 0.9±1.4, n = 355, $p = 3x10^{-28}$, one-sided t-test. Neurons just outside the PPSF (11.5-24.5 µm): z-score = 0.07±0.86, n = 581, p>0.06, one-sided t-test. Neurons located greater than 30 µm away from a target: z-score = -0.08±0.69, n = 4562, $p=1.94x10^{-15}$, one-sided t-test.
c) As, in (a), but for 50-target holograms. Neurons located 0-11.5 µm away from stimulation targets: z-score = 0.28±0.8, n = 265, $p = 3x10^{-8}$, one-sided t-test. Neurons just outside the PPSF (11.5-24.5 µm): z-score = -0.07±0.6, n = 307, p=0.06, one-sided t-test. Neurons located greater than 30 µm away from a target: z-score = -0.08±0.62, n = 2054, $p=2.34x10^{-15}$, one-sided t-test.
d) As, in (a), but for control trials, where the stimulation laser was not engaged. Neurons located 0-11.5 µm away from stimulation targets: z-score = -0.001±0.54, n = 295, p = 0.97, one-sided t-test. Neurons just outside the PPSF (11.5-24.5 µm): z-score = 0.02±0.58, n = 385, p=0.522, one-sided t-test. Neurons located greater than 30 µm away from a target: z-score = 0.04±0.6, n = 1907, p=0.01, one-sided t-test.
e) Scatter plot showing the mean z-scored response of each neuron to each stimulation versus the fano factor of that response (variance / mean). Data are from a representative experiment (N=3 mice) and represent the total response of every target neuron to every light stimulus (n = 710 targets, red dots) or every non-target neuron's response to every stimulus (n = 15,961, black dots). Target neurons were activated more by light than non-targets ($p = 1.58x10^{-321}$, Mann-Whitney U-Test) and were less variable than non-target neurons (p = 0.005, two-sided Mann-Whitney U-Test).
f) As in d, but for control trials. When the stimulation laser was not engaged, target neurons were not modulated more than non-targets (p = 0.53, Mann-Whitney U-test) and their variance around their mean was not significantly different (p = 0.174, two-sided Mann-Whitney U-test)
g) Example maps showing the mean or fano factor of the response to stimulation for all neurons for an example 10-target stimulation. Top, mean response to stimulation targets indicated by green asterisks, columns represent mean images of segmented calcium sources at different depths (see colorbar on right). Bottom, maps showing the fano factor of the Z-scored calcium responses for the same experiment (see colorbar on right). Holographic targets are noted with white asterisks.
h) As in g, but for a control trial where the stimulation was not engaged. Note that neurons do not exhibit strong mean responses in the absence of stimulation, but that variance is similar in control and stimulation trials, consistent with spontaneous activity.

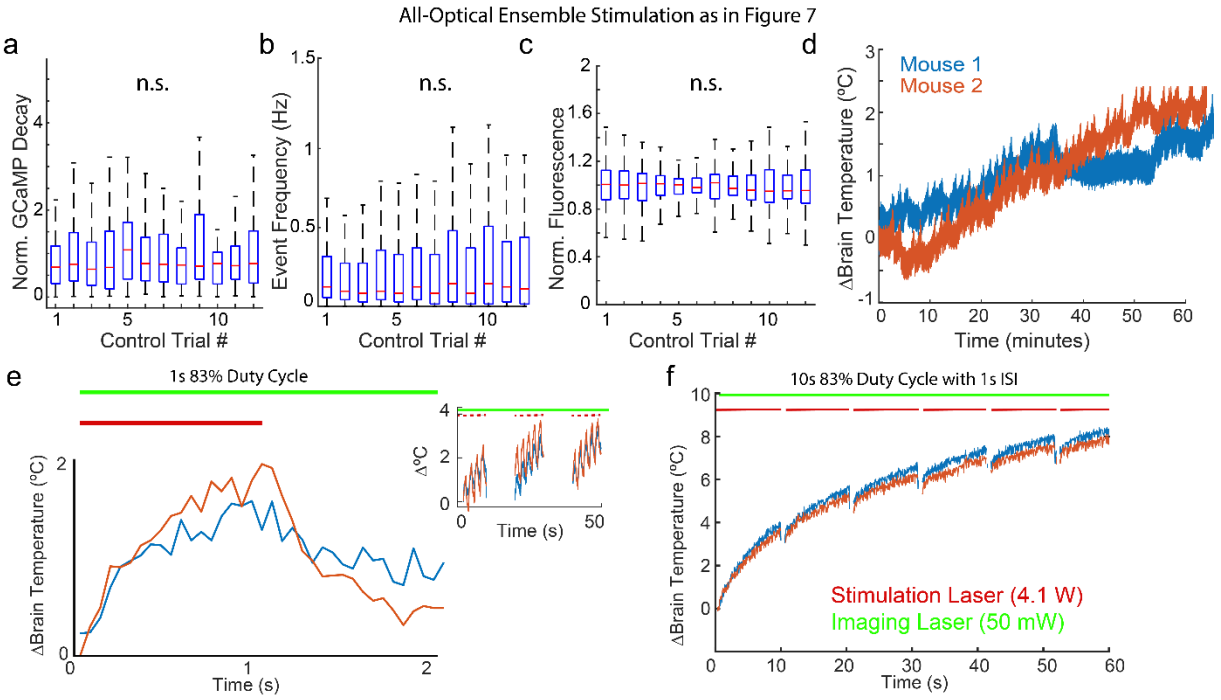

Supplementary Figure 22. Brain heating from all-optical experiments

a) Quantification of GCaMP6s decay tau for successive control trials interleaved with ensemble stimulation trials for experiments shown in Figures 7-8. Control trials were interleaved with 10, 20, and 30 Hz stimulation trials (each trial was 73 seconds long, with a 28 second inter-trial interval, and 33 ensembles were stimulated with ten x 5 ms pulses, with a new ensemble every 2 seconds, while volumetric imaging was being conducted at 930 nm, 50 mW). Data represent the mean normalized decay tau only for neurons targeted for photostimulation (n = 150) during non-stimulation trials. Data represent the median (red line), the 25th and 75th percentiles (blue box) and range (black dotted lines). Statistical significance was assessed by a Kruskal-Wallis test with multiple comparison corrections (p = 0.35).

b) As in (a), but quantifying the spontaneous event frequency for holographic target neurons during control trials interleaved with stimulation trials (p = 0.52).

c) As in (a) and (b) but quantifying the normalized fluorescence intensity of target neurons during interleaved control trials (p = 0.39).

d) Intracranial temperature recordings during an all-optical ensemble stimulation experiment with the same parameters as the experiment shown in figures 7-8, but under anesthesia. Data show temperature recordings from N = 2 mice.

e) Intracranial temperature recording while imaging and stimulating with a fixed 50-target hologram while duty cycling the laser at 83% (2.5 ms on, 0.5 ms off) for one second. Red line indicates when the stimulation laser is engaged, and green line indicates when the imaging laser is engaged. Blue and orange lines represent N = 2 animals. Inset, stimulation is repeated five times a rate of 0.5 Hz, and repeated with a ten second inter-stimulus interval. The resting temperature of the headfixed mouse brain under anesthesia is below physiological temperature (~29° C) due to the water bath and objective functioning as a heat sink.

f) As in e, but for near-continuous stimulation (10 seconds at 83% duty cycle with 1 second inter-stimulus interval).

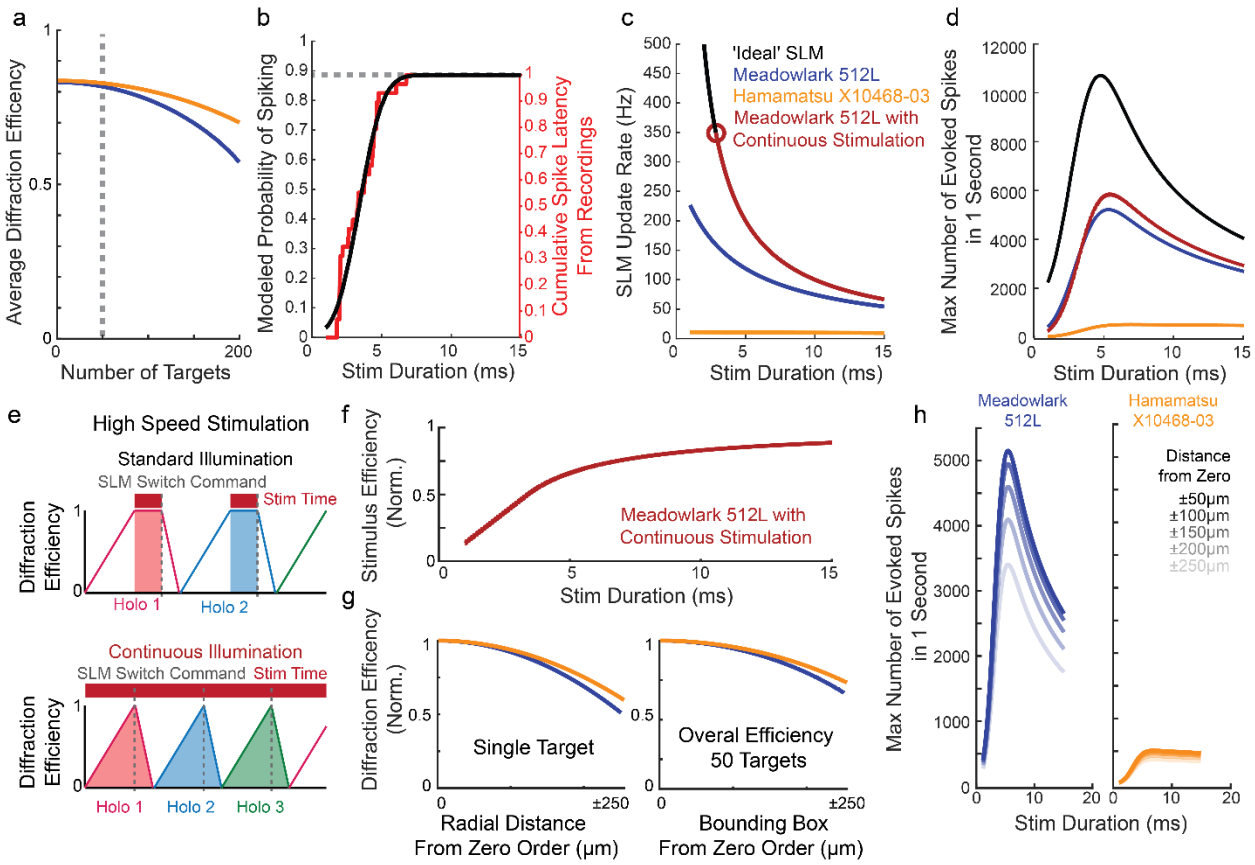

Supplementary Figure 23. Modeling the scale of all-optical ensemble stimulation

a) Simulated diffraction efficiency for two SLMs used in this study (512x512 pixel, Meadowlark 512L *blue,* and 800x600 pixel Hamamatsu X10468-03 *yellow*) displaying holograms with increasing numbers of randomly distributed point targets within the accessible volume. Each value is the average of 1000 simulations. Dotted line: 50 Targets, the reference value used as typical diffraction efficiency of a given SLM.

b) Model of spike probability for arbitrarily short stimuli (*black*). Model is based on the recorded spike latencies from *in vivo* and *ex vivo* recordings (22 neurons latency to fire to 5 ms stimuli, red, right axis). The model is scaled to account for the fraction of cells that were spikeable.

c) The SLM frame update rate as a function of stimulus duration for the two SLMS (blue vs yellow) assuming a blanked hologram during phase transition, or assuming continuous illumination for the Meadowlark 512L (red) or 'Ideal' SLM (black) that has no delay or loss to change phases. Additionally the maximum driver rate for the Meadowlark 512L is noted with an open circle.

d) Estimate for the total number of targets addressable in 1 second with 'ideal' SLM (black), with two different SLMs assuming blanking of transition periods (blue, yellow), or with Meadowlark 512L operated with continuous illumination. Simulation data is the product of the number of stimuli per frame (SLM dependent), by the probability of spiking (b), by the SLM Update Rate (c) all as a function of the stimulus duration. Furthermore, the continuous

illumination strategy is scaled by the stimulus efficiency explained in (f). This model assumes all targets are near the zero order.
e) Schematic of the two illumination strategies modeled. Standard illumination (top) only illuminates holograms when the SLM has completed its phase transition. Therefore, diffraction efficiency is always maximal, but there is a period during phase transitions where no stimulation is occurring. During continuous illumination (bottom) the laser is constantly illuminating the SLM even during phase transitions, but during that transition diffraction efficiency is lower. In both cases the total power that hits different targets is depicted by the shaded area, with the transition command denoted as a dotted line. Continuous illumination is able to go faster but at the expense of efficient stimulation. Note that light that is lost to diffraction in this strategy is directed to the zero order and does not reach the sample (Supplementary Figure 7).
f) Modeled relationship between stimulus duration and mean diffraction efficiency over the entire stimulus period when operating in continuous illumination mode for the Meadowlark 512L SLM. As the diffraction efficiency is low during the middle of phase transition extremely short pulses are inefficient.
g) Diffraction efficiency for both SLMs depend on the radial distance from the zero order. Interpolated diffraction efficiency of a single target hologram (left) placed within the field of view as a function of the radial distance (X and Y axis combined for display). Data is interpolated from measurements of diffraction efficiency of ~1000 individual holograms. Simulation of net diffraction efficiency of a power normalized hologram with 50 targets (right) distributed through a volume bounded radially by the bounding box.
h) The estimate of the largest number of targets addressable in one second with each SLM, and assuming holograms are distributed within one of 5 bounding boxes.

Supplementary Movie 1. SLM performance limitations for high speed 3D-SHOT.
In this experiment, we test 3D-SHOT at the maximal rate of the SLM (~300Hz), and we measure two-photon absorption in space and time during transitions from one SLM frame to another. We consider a sequence of four holograms rapidly displayed in an infinite loop with an external 300Hz trigger clock. Each hologram targets a point cloud randomly distributed in a single focal plane. We measure two-photon absorption with a fluorescent test slide and a substage camera. To measure multiphoton absorption at high speed during this rapid sequence, we synchronize the laser and the SLM clock to only activate the laser at a specific time along the sequence cycle, with a custom phase delay (from 0 to 13.3 ms) and with a 1 ms exposure time. By collecting time-averaged long exposure images with the substage camera for gradually increasing phase delays, we can reconstruct a high speed visualization of the sequence. The red circles indicate the expected target locations considering the frame being displayed on the SLM at any point in time, the image being displayed shows the actual two-photon absorption in the test slide at this same moment. The brightest spot in the center shows light being diffracted in the zero order, which is normally blocked. The movie shows four cycles in a row. Movie is representative of N =2 experiments.

Supplementary Movie 2: All-Optical Ensemble Stimulation in 3D
This movie shows data analyzed in Figures 7-8. The experiments was performed in an awake headfixed mouse free to run on a circular treadmill. 3D-SHOT stimulation targeted ensembles of 10, 25, or 50 neurons located distributed on three imaging planes or on only one focal plane. A new ensemble was stimulated at a rate of 0.5 Hz, and each ensemble was stimulated with ten 5 ms laser pulses at a rate of 30 Hz. Movie shows the pixel-wise z-scored average image of 12 trials, and neuropil signal is subtracted. Magenta arrows appear shortly before the ensemble is stimulated and persist for several frames after stimulation. Movie is representative of N =3 experiments.

Supplementary Table 1: Optical Setup References
In this study, we employed several different optical stimulation paths, as new innovations became available during the course of our research. This table provides specific details on each optical setup and allows the reader to quickly see which figure panels are derived from which optical setups.

Supplementary Table 2: 3D-SHOT 2.0
In this study we present an improved version of 3D-SHOT that employs a rotating diffusor to disperse the geometric focus. This table provides specific parameters and part numbers needed to build both version of 3D-SHOT, as well as a calculation tool that allows users to customize a version of the 3D-SHOT light path suitable for their system.